CERN/PSCC/85-51
PSCC/P88
10 October, 1985

A Proposal for
Tests of Time Reversal and *CPT* Invariance at LEAR.

Zurich:	H.K.Walter, Inst. f. Mittelenergiephysik der E.T.H. A.v.d.Schaaf plus student, Phys. Inst. d. Univ. N.Lordong and W.Bertl, SIN.
C. of William and Mary:	R.Winter and R.Welsh, Dept. of Physics.
U. of Oxford:	N.W.Tanner and E.G.Michaelis, Nuclear Physics, R.H.Dalitz, Theoretical Physics, (theoretical advisor).
U. of New Mexico:	D.Wolfe, N.Komnino, B.Bassaleck, plus two post-doctoral fellows, Dept. of Physics and Astronomy.
Ljubljana:	D.Zavrtanik, A.Stanovnik, M.Mikuz, P.Krizan and G.Kernel, Univ. and Jozef Stefan Inst..
Delft:	H.Postma, H.C.Meijer, W.Lourens, R.W.Hollander and C.W.E.v.Eijk, Technische Hogeschool.
U. of Coimbra:	A.J.P.L.Policarpo and R.Ferreira Marques, Dept. of Physics.
Birmingham:	J.M.Nelson, J.Lowe, S.Hoath and J.D.Davies, Dept. of Physics.

Tests of T and CPT Invariance

Contents

1. Introduction

Given CPT invariance, CP violation and T violation are equivalent. However, although the K° violation of CP has been known for a long time, no experiment has yet demonstrated an explicit T violation and the arguments advanced for CPT invariance are indirect and not altogether unambiguous. The evidence may be summarized quite briefly: There is certainly a difference between the decay curves, shown in Fig.1, for $K^\circ \to \pi^+\pi^-$ and $\bar{K}^\circ \to \pi^+\pi^-$ which is the physical manifestation of the CP violation, but this may be associated with either a T violation or a CPT violation or both. The charge asymmetry of the semileptonic decays, δ_ℓ, adds no clarification as it is consistent with both the T and CPT violating explanations of the $K_{\pi 2}$ decay, and indeed could be due to a CP and CPT violation in the $K_{\ell 3}$ decay itself. Experimentally that is the whole of the existing evidence. At present one can proceed further only by invoking theory in the form of the unitarity relation of Bell and Steinberger[11], which relation requires T violation and is consistent with no CPT violation, although the upper limit which can be placed on the $K^\circ/\bar{K}^\circ$ mass difference, the main test of CPT, is no better than a few percent of the K_S/K_L mass difference[18].

It is entirely possible to resolve the question of T and CPT experimentally and to *measure* the parameters associated with the K° CP violation. The requirement is the comparison of the decay rates of K° and $\bar{K}^\circ$ (strictly neutral kaons which are initially K° and $\bar{K}^\circ$) to various final states as a function of proper time. It is proposed to make the $K^\circ/\bar{K}^\circ$ comparison measurements which would,

(i) determine the complete set of CP parameters, (Re and Im) (ϵ and Δ)

(ii) demonstrate (or refute!) the expected T violation and measure its magnitude to better than 10%,

(iii) test for a direct CP and CPT violation in the $K_{\ell 3}$ decay down to the level of $0.1|\eta_{+-}|$,

and (iv) improve the upper limit on $K^\circ/\bar{K}^\circ$ mass difference to 0.1% of the K_S/K_L mass difference.

The same measurements would incidentally provide,

(v) a better limit for the $\Delta Q = -\Delta S$ amplitude in $K_{\ell 3}$ decays by more than an order of magnitude.

Additional measurements comparing K^+ and K^- decays would

(vi) set a limit on CPT violation from the K^+/K^- lifetime difference of 0.01%.

The LEAR antiproton beam provides a unique opportunity to make precise $K/\bar{K}$ comparisons since stopped $\bar{p}$ annihilating in liquid hydrogen must give equal rates for K and $\bar{K}$ by virtue of the charge conjugation invariance of the strong interaction. The K° and $\bar{K}^\circ$ events are always identifiable by the associated production of K^- and K^+, by conservation of strangeness in the strong interaction. A beam of 10^6 $\bar{p}$ per second at 200 MeV/c focussed to $\sim$ 1mm would provide a near ideal "point" source of K and $\bar{K}$, free of systematic errors and biasses.

Only the decays of kaons to charged particles are considered here. These decays can be identified by low mass detectors and the biasses due to the different strong interactions of particles and antiparticles ($K/\bar{K}$ and π^+/π^-) in the detectors can be minimized. It is proposed to trigger on the decay particles and to make full use of the inherent $K/\bar{K}$ symmetry of the source, subject to small efficiency corrections for particle/antiparticle differences in the detectors.

The theoretical considerations are summarized in Appendix 1 and quoted where necessary in the text as *e.g.* equation (A5).

1.1 Time Reversal Invariance, T.

Probably the best existing tests of T are the limits for

(a) the electric dipole moment of the neutron[2.] $< 6 \times 10^{-25} e$ cm which is still too large to permit significant conclusions to be drawn,

and (b) the transverse polarization of the muon[3] in $K_{\mu 3}$ decay $< 9 \times 10^{-3}$, which is not yet sufficiently sensitive.

The orthodox interpretation of the CP problem predicts[4] a failure of T invariance in the direct form of a failure of detailed balance for the rates $K^\circ \rightarrow \bar{K}^\circ$ and $\bar{K}^\circ \rightarrow K^\circ$ amounting to a difference of $4\,\mathrm{Re}\,\epsilon$, where ϵ is the parameter representing a failure of CP and T invariance (see Appendix I). The T-violation is set out pictorially in Fig. 2 where the $K^-(K^+)$ identifies the initial $K^\circ(\bar{K}^\circ)$, and $e^-(e^+)$ the final $\bar{K}^\circ(K^\circ)$ according to $\Delta Q = \Delta S$. Theoretically the argument is flawed by a possible direct CP and CPT failure in $K_{\ell 3}$ decay, see equation (A9), and experimentally there are considerably advantages in measuring $\mathrm{Re}\,\epsilon$ by means of the comparisons of the decay rates of neutral kaons which are initially K° and $\bar{K}^\circ$,

(a) $K_L \rightarrow \pi^+ e^- \bar{\nu}$, $\pi^- e^+ \nu$, $\pi^+ \mu^- \bar{\nu}$, $\pi^- \mu^+ \nu$ and $\pi^+ \pi^- \pi^\circ$ giving

$$\gamma_L = 2\,\mathrm{Re}(\epsilon + \Delta) \tag{A17}$$

and (b) the integral measurement of $K_S \rightarrow \pi^+ \pi^-$ giving

$$D_{\pi 2} = 2\,\mathrm{Re}(\epsilon - \Delta) + f(\eta_{+-}) \tag{A18}$$

where the integrated interference term $f(\eta_{+-})$ depends on the range of integration but can be calculated from the existing measurements of η_{+-} with an error of $\pm 0.1 \times 10^{-3}$.

The measurement of $D_{\pi 2}$ resolves the ambiguity posed by the possible CP and CPT violation in $K_{\ell 3}$ and allows the direct demonstration of T violation as foreseen by Kabir[4]. The result expected for the $K_{\ell 3}$ test of detailed balance is shown in Fig.4, assuming CPT invariance.

The parameter Δ represents a failure of CP and CPT invariance. At present it is known that $\gamma_L \leq 130 \times 10^{-3}$ and $D_{\pi 2} = (2 \pm 13) \times 10^{-3}$ which are not very useful.

The experimental advantage of measuring the $K^\circ/\bar{K}^\circ$ comparisons of the sum of K_L decays and of $K_S \rightarrow \pi^+\pi^-$ lies in the fact that these measurements are almost totally immune to experimental bias due to the interaction of the particles with the detectors.

1.2 CP Invariance

Unless CPT invariance is simply assumed outright there is the possibility of a direct failure of CP invariance in $K_{\ell 3}$ decays in the form of different decay rates for K° and $\bar{K}^\circ$ to $\pi \ell \nu$. In Appendix I this difference is represented by $\mathrm{Re}\,y_\ell$ for the $\Delta S = \Delta Q$ decays and $\mathrm{Re}(x_\ell - \bar{x}_\ell)$ for $\Delta Q = -\Delta S$, which parameters appear in the expression for the lepton asymmetry

$$\delta_\ell = 2\,\mathrm{Re}(\epsilon - \Delta) - \mathrm{Re}(y_\ell + x_\ell - \bar{x}_\ell) \tag{A13}$$

Now $2\,\mathrm{Re}(\epsilon - \Delta)$ is determined by $D_{\pi 2}$ as discussed in the previous section, and δ_ℓ itself is known quite accurately[8], $\delta_\ell = (3.30 \pm 0.12) \times 10^{-3}$, so the $K_{\ell 3}$ CP violation would be obtained without further measurement.

Additional measurements of the various $K_{\ell 3}$ rates in the region of K_S/K_L interference, $\Gamma_S t \simeq \pi$, can determine $\mathrm{Re}\, y_\ell$ and $\mathrm{Re}(x_\ell - \bar{x}_\ell)$ separately (see Appendix I).

It should be remarked that the familiar failure of CP invariance, Fig. 1, has never been demonstrated by direct comparison of K° and $\bar{K}^\circ$. The difference in the region of $\Gamma_S t \sim 14$ is quite gross and eminently measurable with a $\bar{p}p$ source. In fact the $\pi^+\pi^-$ decays in this region of $\Gamma_S t$ represent a significant and asymmetric background to the K_L measurements.

The failure of CP invariance expected in $K_{\pi 3}$ decays, $\eta_{+-\circ}$ in equation (A15), gives a $K^\circ/\bar{K}^\circ$ difference which is $\leq 2\,\mathrm{Re}\,\eta_{+-\circ}$, and of this magnitude only for $\Gamma_S t \lesssim 1$, which is practically out of range for the kaon momenta from $\bar{p}p$ annihilations. Furthermore the $K_{\pi 2}$ background is very large and asymmetric, and for $\eta_{+-\circ} \simeq \eta_{+-}$ the $K_{\pi 3}$ difference will be near zero.

1.3 CPT Invariance

CPT invariance requires[9)] equal masses and decay rates for particles and antiparticles, but a difference can occur only if both CPT *and* CP fail[10)], which focuses attention on the $K/\bar{K}$ system. The parameter Δ in Appendix I is related to the mass and width differences of K° and K°,

$$\frac{M - \bar{M}}{M_L - M_S} \simeq 2(\mathrm{Im}\Delta - \mathrm{Re}\Delta); \quad \frac{\Gamma - \bar{\Gamma}}{\Gamma_S - \Gamma_L} \simeq 2(\mathrm{Im}\Delta + \mathrm{Re}\,\Delta) \qquad (A20)$$

which, because of the small denominators, constitute very sensitive tests for CPT invariance. $\mathrm{Re}\,\Delta$ would be determined, together with $\mathrm{Re}\,\epsilon$, from the $K/\bar{K}$ difference measurements γ_L and $D_{\pi 2}$, equations (A17) and (A18), discussed in paragraph 1.2 in connection with T-invariance.

For $\mathrm{Im}\Delta$ it is necessary to determine the $K_{\ell 3}$ decay rates in the region of K_S/K_L interference, in particular the quantity α_ℓ, equation (A8), which is the fractional difference of the rates for an initial $\bar{K}^\circ$ eventually decaying to $\pi^+e^-\bar{\nu}$ and an initial K° eventually decaying to $\pi^-e^+\nu$. The proper time dependence of α_ℓ is shown in Fig. 3 for $\mathrm{Re}\,\Delta = x_\ell = \bar{x}_\ell = 0$. Other $K_{\ell 3}$ differences in the interference region determine the $\Delta Q = -\Delta S$ amplitudes x_ℓ and $\bar{x}_\ell$, and $\mathrm{Re}\,\Delta$ is determined by the measurements of γ_L and $D_{\pi 2}$ (see Appendix I).

At present no useful limit can be placed on the mass and width differences[18)] of K° and $\bar{K}^\circ$ without making assumptions additional to those in Appendix I. If hermiticity is assumed and the unitarity relation of Bell and Steinberger[11)], equation (A21), employed then the limit obtained is

$$\left|\frac{M - \bar{M}}{M_L - M_S}\right|, \left|\frac{\Gamma - \bar{\Gamma}}{\Gamma_S - \Gamma_L}\right| \lesssim 26 \times 10^{-3}$$

due to the present uncertainty of $D_{\pi 2}$ (see section 1.2). The $K^\circ/\bar{K}^\circ$ comparisons proposed here are capable of reducing the limit to 10^{-3} without invoking hermiticity.

A numerically better limit for CPT can be provided by the difference of K^+ and K^- lifetimes. In a kaon beam measurement limited by systematic errors Lobkowicz et al[13)] obtained

$$\left|\frac{\Gamma_+ - \Gamma_-}{\Gamma_+ + \Gamma_-}\right| < 1.5 \times 10^{-3}$$

which is open to improvement using the two body annihilation channel $\bar{p}p \to K^+K^-$ at LEAR by approximately an order of magnitude.

1.4 The $\Delta Q = \Delta S$ Rule

It is believed that in $K_{\ell 3}$ decays the $\Delta Q = -\Delta S$ amplitude x_ℓ for $K^\circ \to \pi^+ e^- \bar{\nu}$, will be $\sim 10^{-14}$ smaller than the $\Delta Q = \Delta S$ amplitude for $K^\circ \to \pi^- e^+ \nu$, but the present limit is hardly better than 10^{-1}. For $\Gamma_S t \sim 1$ the various $K^\circ/\bar{K}^\circ$ differences for $K_{\ell 3}$ decays are sensitive to $\Delta Q = -\Delta S$ amplitudes x_ℓ for K° and $\bar{x}_\ell$ for $\bar{K}^\circ$. The interesting case is β_ℓ, equation (A9), which for $|x_\ell|$, $|\bar{x}_\ell| \ll \frac{1}{2}\Gamma_S t \ll 1$ has the form $\beta_\ell = \{\mathrm{Im}(x_\ell + \bar{x}_l) - \mathrm{Re}(x_\ell - \bar{x}_\ell)\}/\frac{1}{2}\Gamma_S t$ which is shown in Fig. 4 for $\mathrm{Re}(x_\ell - \bar{x}_\ell) = 0$, *i.e.* CPT invariance, and $\mathrm{Im}x_\ell = 5.6 \times 10^{-3}$ which is one tenth of the present experimental limit. Such a failure of the $\Delta Q = \Delta S$ rule would be clearly recognized in the proposed measurements.

1.5 Summary of K° Measurements

The measurements proposed include

(a) the sum of the K_L decays $\pi^\pm e^\mp \nu$, $\pi^\pm \mu^\mp \nu$ and $\pi^+\pi^-\pi^\circ$ for $\Gamma_S t \gtrsim 2\pi$,
(b) the K_S decay to $\pi^+\pi^-$,
(c) the separate $K_{\ell 3}$ decays, $\pi^+ e^- \bar{\nu}$ and $\pi^- e^+ \nu$, for $\Gamma_S t \lesssim 2\pi$,

in each case identifying the initial K° or $\bar{K}^\circ$ by detecting the associated K^- or K^+ from the $\bar{p}p$ annihilation. This set of measurements, together with the properties of neutral kaons already known accurately, would be sufficient to determine directly *all* the parameters of the K° problem, (Re and Im) (ϵ and Δ), and to establish the status of T and CPT invariance, and of CP invariance in the case of $K_{\ell 3}$ decays. The test of $\Delta Q = \Delta S$ would be a by-product of these measurements. A sample of the separate $K_{\ell 3}$ decays, $\pi^+ e^- \bar{\nu}$ and $\pi^- e^+ \nu$, for $\Gamma_S t \gtrsim 2\pi$ could establish a failure of detailed balance.

2. The Apparatus

The solenoid magnet and detectors are shown in Figs. 5 and 6, and some details of the central region in Fig. 7. The cylindrical chambers and scintillator hodoscope subtend a solid angle of $0.86 \times 4\pi$ steradian at the liquid hydrogen target, and divide the cylindrical space into four annular regions which can be specified in terms of the cylindrical polar radius R:

$R < C_4 = 2$cm, $\bar{p}p$ annihilation source
$C_4 < R < C_{20} = 10$cm, K_S decays, K°_{l3} interference region
$C_{20} < R < C_{100} = 50$cm, K_L and $K^\pm$ decays, $K^\circ_{\pi 2}$ interference region
$C_{100} < R < coil = 95$cm, Decay tracks.

The scintillator hodoscope is at $R = 90$cm and is 3m long.

The important features of the apparatus are

(i) a minimum of mass, particularly in the decay regions, to avoid the asymmetries due to strong interactions of particles and the background due to e^+e^- pairs from γ-ray conversions,
(ii) good time-resolution for the hodoscope and the beam scintillator as the principal means of particle identification,
(iii) sufficient track information to permit the reconstruction of momenta and vertices, and to provide kinematic checks,
(iv) simplicity of geometry which permits rapid analysis of data.

2.1 Antiproton Beam and Target (Figs. 5 and 7)

The LEAR antiproton beam is entirely free of contamination by other particles and is contained within a transverse phase space of $\sim 10\pi$ mm $\times$ mm with a momentum spread of 0.1%. At 200 MeV/c (20 MeV kinetic energy) such a beam can be focussed through a degrader, which reduces the momentum to 100 MeV/c (5 MeV K.E.), to annihilate $\sim$ 3mm inside a liquid hydrogen target in a volume of $\sim$ 1mm^3. It is proposed to use a degrader made up of a 1mm thick Be window for the machine vacuum and a 2mm thick beam scintillator. The light output from the slow $\bar{p}$ in this scintillator is equivalent to minimum ionizing particles in $\sim$ 4cm of scintillator.

A small beam focus, $\sim$ 1mm, requires a quadrupole lens pair or triplet *inside* the magnet. It is proposed to use either an electrostatic lens or a magnetic lens equipped with a counter-winding carrying the same current as the solenoid to avoid disturbing the uniformity of the field.

The liquid-hydrogen cell (Fig. 7) is envisaged as a mylar tube 5mm diameter $\times$10mm long with an inner mylar tube of 4mm diameter to provide a flow and return system for condensing liquid. The axial, Z, position of the $\bar{p}$ annihilation volume can be controlled through the beam momentum, and the transverse position by biassing the quadrupole. The distribution of the $\bar{p}p$ annihilation points is monitored by the particle detecting equipment. In the event of an unfavourable beam halo it may be necessary to trim the phase space upstream of the apparatus.

2.2 The Magnet (Fig. 5)

It is proposed to use the Jade magnet, now installed at DESY, modified to accommodate a hodoscope of 128 scintillators. This magnet is a solenoid which provides a field of up to 0.5 Tesla, uniform to 0.7%, over a volume 1.8m diameter and 3.5m length. For this experiment it would be run at half power, $\sim$ 1MW, with a field of 0.3 Tesla since the decay particles have low momenta. The total weight of the magnet is $\sim$ 110 tons and its volume is approximately (4m)^3.

It is extremely desirable to reverse the magnetic field between LEAR beam spills so that any mechanical asymmetries can be averaged out. Reversing the field is more or less equivalent to charge conjugation, $K^\pm \rightarrow K^\mp$ and $\pi^\pm \rightarrow \pi^\mp$. In fact mechanical asymmetries lead to $K/\bar{K}$ asymmetries only through rather obscure second order effects which are not expected to be large, but there is no obvious way of checking for these asymmetries except by reversing the field.

2.3 Particle Detectors

C_4, Fig. 7, is a cylindrical multi-wire proportional chamber 8cm long with 128 anodes on a 36mm diameter, 0.9mm pitch, and a 6mm cathode to cathode spacing. To minimize the mass it is proposed to use aluminized mylar for the outer window and to support it with 128 Kevlar threads.

C_{20}, Fig. 7, is a cylindrical multi-wire proportional chamber, 40cm long, with 512 anodes on a nominal 20cm diameter, 1.2mm pitch, and cathode strips for the purpose of providing a pick-up signal for determining the Z-coordinates.

C_{100}, Figs. 5 and 6, is a 1m diameter by 2m long multi-wire proportional chamber with 1024 anodes and cathode strip pick-up to determine the Z-coordinates.

The *Drift Chamber*, Figs. 5 and 6, has 105 sectors each containing 7 anodes, at radii between 55.5 and 79.5cm and of length 3m, making a total of 735 approximately square cells, with sides of about 4cm and drift times up to $\sim$ 400ns. The maximum drift time of interest is less than 512ns which permits the use of the Lecroy 4290 read-out system with 1ns resolution. It is, however, proposed to modify this system to allow the recording of two hits on one wire within 512ns.

C_{170}, Figs. 5 and 6, is a 1.7m diameter by 3m long multi-wire proportional chamber with 1024 anodes and cathode strip pick-up to determine the Z-coordinates.

The *Scintillation Hodoscope*, Figs. 5 and 6, has 128 scintillator strips each 43mm square forming a cylinder of 1.8m diameter and 3m length. Each scintillator is equipped with two photomultipliers which are read out to ADC's and TDC's.

2.4 The Decay Volume and Materials

For K_L and $K^{\pm}$ decays the decay volume extends from C_{20} to C_{100} and it is necessary to minimize the hadron interactions and the gamma conversions. Helium is the only practical choice since, apart from safety considerations, hydrogen suffers from an inconvenient π^+/π^- difference.

The radial (cylindrical polar) thickness of the helium plus the windows and gas of C_{20} outside the outer layer of wires amounts to $\sim 2.1 \times 10^{-4}$ radiation length (He 0.76, Mylar 0.84, A 0.55) or $\sim$ 14mg/cm^2 (He 10, Mylar 3, A 1) of which 0.14mg/cm^2 is hydrogen.

For K_S decays and K_{l3} interference effects the interesting volume is between C_4 and C_{20}. Radially there is $\sim 3 \times 10^{-5}$ radiation length or $\sim$ 2mg/cm^2 including the exit window from C_4 but not the entrance window to C_{20}. (Air between C_4 and C_{20} would increase the mass to $\sim$ 9mg/cm^2, $\sim 2.5 \times 10^{-4}$ radiation length).

The large masses in the apparatus are the drift chamber and C_{170} ($\sim$ 75mg/cm^2, $\sim 4 \times 10^{-3}$ radiation length), the chamber casing ($\sim$ 2.5g/cm^2, $\sim$ 0.1), the scintillators (4.4g/cm^2, $\sim$ 0.1) and the coil ($\sim$ 20g/cm^2, $\sim$ 1). At the centre there is, radially, $\sim$ 20mg/cm^2 of liquid hydrogen and mylar ($\sim 3\times10^{-4}$ radiation lengths) and 54mg/cm^2 of aluminium (22.5×10^{-4}).

3. The Trigger and Backgrounds

The annihilation $\bar{p}p$ gives the following products[14)]

$n\pi^\circ, n > 2$	3.2%	
$\pi^+\pi^-$	0.3	
$\pi^+\pi^- n\pi^\circ, n > 0$	42.2	
$2(\pi^+\pi^-)n\pi^\circ, n \geq 0$	45.6	
$3(\pi^+\pi^-)n\pi^\circ, n \geq 0$	3.8	
Total pionic	95.3	
$K\pi K = K^-\pi^+K^\circ + K^+\pi^-\bar{K}^\circ$	0.42	
$K\pi K\pi = K^-\pi^+K^\circ\pi^\circ + K^+\pi^-\bar{K}^\circ\pi^\circ$	0.92	($K^\circ/\bar{K}^\circ$ events
$K\pi K2\pi = K^-\pi^+K^\circ 2\pi^\circ + K^+\pi^-\bar{K}^\circ 2\pi^\circ$	0.13	of interest.)
Sub-Total $K^\pm\pi^\mp K^\circ(n\pi^\circ)$	1.47	
K^+K^-	0.1	
$K^+K^- n\pi^\circ, n > 0$	0.64	
$K^\circ\bar{K}^\circ n\pi^\circ, n \geq 0$	0.65	
$K^\circ\bar{K}^\circ\pi^+\pi^- n\pi^\circ, n = 0, 1$	1.15	
$K\bar{K}$, 4 charged	0.86	
Total kaonic	4.87	

On average there are 3 charged particles and about 4γ-rays per $\bar{p}p$ annihilation. For $K^\pm\pi^+K^\circ n\pi^\circ$ the average value n is 0.80, i.e. 1.6 γ per event. At 10^6 $\bar{p}$ per second there would be $\sim 2 \times 10^6$ tracks per second within the solid angle $\Delta\Omega = 0.86 \times 4\pi$ of the apparatus, and a 5% probability of two $\bar{p}p$ annihilations within the 50ns gating time of the multi-wire proportional chambers. It is proposed to veto triggers for which the beam scintillator receives two anti-protons, arriving within 50ns, and to record the time of arrival of any anti-protons arriving within $\pm$512ns.

Generally the triggers are based on multiplicity measurements supplemented by hit correlations for the proportional chambers, and time of flight from the beam scintillator to the hodoscope. Multiplicity discriminates heavily against pionic annihilations since the kaon decays of interest (apart from the special case of K^+K^- collinear pairs) increase the number of charged particles by two.

The $\bar{p}p$ annihilations to $K^{\pm}\pi^{\mp}K^{\circ} + K^{\pm}\pi^{\mp}K^{\circ}\pi^{\circ} + K^{\pm}\pi^{\mp}K^{\circ}2\pi^{\circ}$ followed by a K° decay outside C_{20}, the K_L region, give a multiplicity pattern

$$C_4 = C_{20} = 2 \qquad C_{100} = C_{170} = 4$$

where C_x means the multiwire proportional chamber of x cm diameter. For K_0 decays inside C_{20} the pattern is

$$C_4 = 2 \qquad C_{20} = C_{100} = C_{170} = 4$$

The trigger system is shown schematically in Fig. 8. It starts with the detection of an antiproton by the beam scintillator S_0, and the level 1 trigger is formed by the coincidence of this signal with a multiplicity trigger.

The multiplicity signals for each of the wire chambers are formed by an existing hardware device called the Combination and Multiplicity Unit (C.M.U.). This accepts the Prompt OR outputs from the PCOS III Delay and Latch Units (LRS 2731), combines signals on adjacent inputs to give one signal, and generates an output indicating the multiplicity of signals for the (combined) input from each chamber. The PCOS III Prompt OR, which is undelayed and unlatched, pairs the wires of the chambers but this does not constitute a significant loss for the multiplicity trigger.

The Programmable Logic Unit (PLU) receives the statements of the multiplicity for each of the chambers and the hodoscope and may be programmed to accept the pattern 2244 for K_L decays, 2444 for K_S decays, and others as required. All of these trigger patterns may be considered at the same time, with a topology word generated by the PLU to identify which type of trigger actually occurred. If the pattern is accepted the PLU generates a "go" signal about 200ns after the event.

The Level 1 (multiplicity) trigger latches the PCOS hits and also begins the encoding of the scintillator times and pulse heights from the TDC and ADC system which is the slowest part of the trigger process.

The PCOS electronics latches all of the wire chamber hits, and the scintillator hits as well. The hit wire/scintillator numbers, in the form of a mean wire number and cluster size, are read via the ECL Bus Port on the PCOS controller at 10 MHz into the 4302 memory of a CAB trigger processor BG*. The CAB then starts a search for two candidates for trajectories emanating from the $\bar{p}p$ source by correlating the hits on C_4, C_{20}, C_{100}, C_{170} and S_c within a prescribed range of possibilities recorded in a look-up table. Given the value of the magnetic field one can use another look-up table to find the transverse momentum p_T, directly. The CAB look-up procedures take about 100μs. If at the end of this stage, Level 2, suitable trajectories are identified then the TDC and ADC information, which is available 60 to 100μs after the Level 1 trigger, is read by the CAB BG* which is on the CAMAC Branch Highway. The CAB carries out the pedestal and walk corrections for the scintillator times using look-up techniques in the CAB readable memory, and calculates by straight forward arithmetic the quantity t_0 given by,

$$4t_0^2 = (t_1 + t_2)^2 - \beta^2 (t_1 - t_2)^2$$

where $\beta = v/c \simeq \frac{1}{2}$ is the propagation velocity in the scintillator, t_1 and t_2 are the times, duly corrected, recorded at the two ends of one scintillator, and t_0 is the time of flight for the particle travelling perpendicular to the axis of the detectors with the observed transverse momentum p_T. The expression for t_0 is exact. The quantity t_0 can be compared, via a look-up table with the expected value for a pion or a kaon mass since p_T has already been determined during Level 2 processing. A trigger is then accepted at this Level 3 if one of the identified trajectories emanating from the $\bar{p}p$ source has a t_0 consistent with a kaon and the other a t_0 consistent with a pion. Level 3, which completes the triggering, brings the total time from the $\bar{p}$ arrival to about 200μs, although a rejection at any one of the three Levels will cause the system to abort, clear, and restart at the time of the rejection.

If an event is accepted at Level 3 then all the pertinant information is transferred to a second CAB, CG^x, see Fig.9, which collects and buffers it. This CAB acts as Crate Controller and it can transfer highly compressed packets of data to a VAX (e.g. for storage on tape, laser disk, etc.). The auxillary crate, Fig.9, contains memories, data registers, and various crate controllers. There is an A_2 controller to access the VAX and another connected to a PDP 11/60 whose function is regularly to check the timing characteristics of the scintillators. This calculation involves firing light pulsers as well as using $\bar{p}p$ annihilation events to recalculate pedestals, etc., and down-loading these numbers into the CAB memories. The auxillary crate also contains a GPIB controller connected to a HP9826 used for controlling and monitoring during data taking.

Most of the trigger processing hardware and software described here already exists and has been used successfully in previous experiments.

3.1 K_L Triggers

For neutral kaon decays between C_{20} and C_{100} the multiplicity trigger required is

$$C_4 = 2 \qquad C_{20} = 2 \qquad C_{100} = 4 \qquad C_{170} = 4$$

Such a 2, 2, 4, 4 pattern can also be generated by

(a) $\bar{p}p \rightarrow \pi^+\pi^-\pi^\circ$ etc and a γ conversion between C_{20} and C_{100} yielding a $\pi^+\pi^-e^+e^-$ event,

(b) $\bar{p}p \rightarrow \pi^+\pi^-$ etc and the back-scatter of a pion by the coil, and

(c) a variety of other kaon decays.

The trigger probabilities have been calculated for a geometric solid angle of $\Delta\Omega/4\pi =$ 0.86 and a magnetic field $B = 0.3$ Tesla allowing inefficiencies per particle of 3% per wire chamber. Losses of good triggers due to two particles entering one or adjacent sectors of C_{170} (16%) and decays of $K^\pm$($\sim$ 30%) have also been considered. The number of triggers expected for 10^6 $\bar{p}p$ annihilations is given in Table I for each Level of the trigger. No deductions have been made for the dead-time losses, but the dead time associated with each Level is indicated in parenthesis.

Table I

K_L Triggers 2, 2, 4, 4

Annihilation Channel	Level 1 (0.1μs)	Level 2 (100μs)	Level 3 (200μs)
$K^{\pm}\pi^{\mp}K^{\circ}(n\pi^{\circ})$			
$K^{\circ} \rightarrow \pi e\nu + \pi\mu\nu + \pi\pi\pi$	70	50	50
$K^{\circ} \rightarrow \pi^{+}\pi^{-}$	16	12	12
$K^{\pm} \rightarrow \pi^{\pm}\pi^{+}\pi^{-}$	20	~ 0	~ 0
$K^{+}K^{-}(n\pi^{\circ})$	28	~ 0	~ 0
$K^{\circ}\bar{K}^{\circ}(n\pi^{\circ})$	16	16	~ 0
$K^{\circ}\bar{K}^{\circ}\pi^{+}\pi^{-}$	82	82	~ 0
$\pi^{+}\pi^{-}(n\pi^{\circ})$			
$\pi^{+}\pi^{-}e^{+}e^{-}$	196	196	~ 0
Backscatters	78	78	~ 0
Total	506	434	62

3.2 K_S Triggers

The multiplicity pattern for neutral kaon decays between C_4 and C_{20} is 2, 4, 4, 4 which can be simulated by

(a) $\pi^{+}\pi^{-}e^{+}e^{-}$ events arising from a γ-conversion between C_4 and C_{20}, *or* a small angle Dalitz or γ-converson pair inside C_4 and C_4 inefficiency (much the most important source).

(b) $\pi^{+}\pi^{-}$ backscatters,

and (c) a variety of other kaon decays.

The number of triggers expected for 10^6 $\bar{p}p$ is given in Table II where allowance has been made for the geometric, inefficiency, and decay losses, but not dead time losses.

Table II

K_S Triggers 2, 4, 4, 4

Annihilation Channel	Level 1 (0.1μs)	Level 2 (100μs)	Level 3 (200μs)
$K^{\pm}\pi^{\mp}K^{\circ}(n\pi^{\circ})$			
$K^{\circ} \rightarrow \pi e\nu$	7	5	5
$K^{\circ} \rightarrow \pi\mu\nu + \pi\pi\pi$	7	5	5
$K^{\circ} \rightarrow \pi^{+}\pi^{-}$	410	290	290
$K^{\pm} \rightarrow \pi^{\pm}\pi^{+}\pi^{-}$	3	~ 0	~ 0
$K^{\circ}\bar{K}^{\circ}(n\pi^{\circ})$	80	80	~ 0
$K^{\circ}\bar{K}^{\circ}\pi^{+}\pi^{-}$	400	400	~ 0
$K^{+}K^{-}(n\pi^{\circ})$	3	~ 0	~ 0
$\pi^{+}\pi^{-}(n\pi^{\circ})$			
$\pi^{+}\pi^{-}e^{+}e^{-}$	250	250	~ 0
Backscatters	3	3	~ 0
	1163	1033	300

It would not be difficult to add a Level 4 trigger which would identify $K^{\circ} \rightarrow \pi^{+}\pi^{-}$ decays by invariant mass, using a look-up table procedure, so that a less dilute K_{e3} sample could be recorded.

3.3 K^+K^- Trigger

The K^+K^- events of interest are characterized by a collinear pair of 800 MeV/c, with one but not both kaons decaying between C_{20} and C_{100}. A hardware change is necessary for this trigger, the Combination and Multiplicity Unit of Fig.8 being replaced by a Collinearity Unit fed from the Prompt OR output of PCOS III. The collinearity unit and the PLU impose the requirement of diametrically opposite hits on C_4 and on both the wires and the cathode strips of C_{20}, and *no* diametrically opposite hits on C_{100}. Here "diametrically opposite" is to be understoood to include a correction for the curvature of the 800 MeV/c trajectories in the magnetic field. Given this Level 1 trigger the CAB BG* verifies the multiplicity pattern

$$C_4 = C_{20} = C_{100} = C_{170} = 2$$

and searches for a correlation of hits on C_4, C_{20}, C_{100}, and C_{170} consistent with a single trajectory of 800 MeV/c emanating from the source, Level 2. On receipt of the ADC and TDC information from the scintillators the CAB checks the momentum and T.o.F., using look-up tables, for the single trajectory. The number of triggers expected for 10^6 $\bar{p}p$ annihilations is given in Table III where allowance has been made for chamber inefficiencies and particle decays, but not dead time.

Table III

K^+K^- Triggers 2, 2, 2, 2

	Level 1 (0.1μs)	Level 2 (100μs)	Level 3 (200μs)
K^+K^-, one decaying	105	100	100
K^+K^-, no decay	40	~ 0	~ 0
$\pi^+\pi^-$ collinear	140	5	~ 0
$\pi^+\pi^-$ spatial randoms	90	~ 0	~ 0
	375	105	100

3.4 Calibration Triggers

(a) Cosmic Rays
Multiplicity pattern $C_{100} = C_{170} = 2$
Rate $\sim 200\ \mathrm{s}^{-1}$.
The purpose of this trigger is the determination of the drift chamber parameters and other tests without beam.

(b) $\bar{p}p \to \pi^+\pi^-$ and K^+K^-, collinear pairs.
Multiplicity pattern $C_4 = C_{20} = C_{100} = C_{170} = 2$, strobed by a coincidence between opposite ends of "diametrically opposite" scintillator strips, with due allowance for the curvature of the trajectories of the 926 MeV/c $\pi^+\pi^-$ pairs and 800 MeV/c K^+K^- pairs.
For 10^6 $\bar{p}p$, 1950 $\pi^+\pi^-$ triggers and 450 K^+K^- triggers are expected which will provide the calibration for the times and pulse heights of the scintillators from which times of flight are extracted. Typically the $K^\pm$ time of flight is 0.6ns longer than $\pi^\pm$ for the collinear pairs.

(c) K^+ decay to $\mu^+\nu$ or $\pi^+\pi^\circ$
The decay of a *stopped* K^+ would be signalled by a hit on the hodoscope delayed by about 10ns, and this is expected for several percent of the kaon triggers i.e. a few K^+ decay triggers per 10^6 $\bar{p}p$. The stopped K^+ provide monochromatic μ^+

and π^+ of 236 and 205 MeV/c respectively which are valuable for calibrating the momentum resolution.

(d) $\bar{p}p \to K^{\pm}\pi^{\mp}K^{\circ}(n\pi^{\circ})$, $K^{\circ} \to \pi^+\pi^-$, $K^{\pm} \to \pi^{\pm}\pi^+\pi^-$
A multiplicity trigger 2, 4, 6, $\geq$ 4, i.e.

$$C_4 = 2 \qquad C_{20} = 4 \qquad C_{100} = 6 \qquad C_{170} \geq 4,$$

selects these events and permits the determination of the inefficiency of C_{170} and the hodoscope for decay $\pi^{\pm}$, including the loss due to interactions between C_{100} and C_{170}. Similarly a multiplicity pattern 2, 4, $\geq$ 4, 6 measures the inefficiency of C_{100}. The number of triggers expected is 1.6 per 10^6 $\bar{p}p$, of which 28% are due to $\bar{p}p \to K^{\pm}\pi^{\mp}K^{\circ}$ and are kinematically complete.

3.5 Data Recording

It would be convenient to record only a one third sample of the K_S triggers involving a K_{π_2} decay, and a 1% sample of calibration (b), $\pi^+\pi^-$ and K^+K^-. The total numbers of triggers under these conditions is given in Table III.

Table IV

Trigger Summary

Trigger	No per $10^6\bar{p}p$
$K_L : K_{e3} + K_{\mu 3} + K_{\pi 3}$	50
$K_{\pi 2}$	12
$K_S : K_{e3}$	5
$K_{\mu 3} + K_{\pi 3}$	5
$K_{\pi 2}$, $\frac{1}{3}$ sample	100
K^+K^-	100
Calibration	28
Total	300

Typically one event record requires about 350 bytes giving $\sim 2 \times 10^5$ events (equivalent to $7\times10^8\bar{p}p$) per 6250 bpi tape, and 6×10^6 events (equivalent to $\sim 2\times10^{10}\bar{p}p$) per laser disk.

4. Identification of Events

The analysis programme is presented with the drift chamber data and the cathode strip information from C_{20}, C_{100} and C_{170}, in addition to the anode information from the proportional chambers and the times and pulse heights from the scintillators which are used for the trigger. After decoding the search for hit correlations indicative of particle trajectories and the extraction of times of flight is repeated with greater accuracy making use of the ϕ-coordinates from the drift chamber and the z-coordinates from the proportional chambers. Both the trajectories emanating from the $\bar{p}p$ source and those from a possible decay are obtained, and the source vertex and decay vertex coordinates reconstructed. Given, in the case of K° triggers, four trajectories and two vertices which are acceptable and no stray tracks which interfere, the event can be reduced to (a) the $\bar{p}p$ source point, two momentum vectors, and two times of flight, and (b) the decay vertex coordinates, two momentum vectors, and two times of flight. The K^+K^- and calibration triggers can be similarly reduced.

4.1 $K^{\pm}\pi^{\mp}$ Pairs

For accepted events the momentum distributions for the particles depend markedly on the lifetime of the K° decay. Fig.10 shows the distribution of K° momenta for events involving K_L and K_S decays. The corresponding $K^{\pm}$ momentum spectrum for events with a K_L decay, the more difficult case for $K^{\pm}$ identification, is shown in Fig.11.

The identification of $K^{\pm}$ against a background of $\pi^{\pm}$ is provided by the time of flight difference $\Delta t = t_K - t_\pi$, where t_K and t_π are the K and π times of flight for the same momentum and trajectory. The probability distribution for Δt derived from the $K^{\pm}$ momentum of Fig.11 is shown in Fig.12(a). The minimum time difference is 0.6ns. This requires good time of flight resolution but is clearly within the range of existing technology with a favourable calibration source, $\bar{p}p \rightarrow \pi^+\pi^-$, and little time jitter from the beam scintillator.

The $K^{\pm}\pi^{\mp}$ identification by T.O.F. is subject to a number of kinematic checks. Some 28% of the events, about a quarter for K_L decays and a third for K_S decays, are due to annihilations $\bar{p}p \rightarrow K^{\pm}\pi^{\mp}K^\circ$ which can be recognized by the position of the decay vertex relative to the $K^{\pm}$ and $\pi^{\mp}$ momentum vectors. For these events the $K^{\pm}\pi^{\mp}$ missing mass is predicted to have a spectrum as shown in Fig.13. For the more numerous $K^{\pm}\pi^{\mp}K^\circ\pi^\circ$ events the $K^{\pm}$ and $\pi^{\mp}$ momenta and the decay vertex position determine the K° momentum and the missing (π°) mass.

In all cases the distinction between a $K^+\pi^-$ event and a $K^-\pi^+$ event is quite clear. A false identification of a $K^+\pi^-$ event as $K^-\pi^+$ leads to a time difference error of at least 1.6ns and usually much greater as shown in Fig.12(b).

4.2 K_{e3} Decays $< C_{20}$

The momenta of the electrons from $K^\circ \rightarrow \pi e\nu$ decays, Fig.14, are low enough and the flight path from decays within C_{20} long enough to permit the distinction between electrons and pions by time of flight. Fig.15(a) gives the integral probability distribution for decay trajectories, with the momentum distribution of Fig.14, to have a π/e time of flight difference $> \Delta t = t_\pi - t_e$. For a time resolution which recognizes a 0.5ns difference 85% of the electrons of K_{e3} decays can be identified by time of flight, making the necessary correction for the K° time of flight. The distinction between the true interpretation of a K_{e3} decay as, say, π^+e^- and the false interpretation as π^-e^+, Fig.15(b), is a time difference > 0.6ns for 99.5% of all events and > 1.1ns for the 85% of events identified by electron time of flight. Using the same methods about half of the $K_{\mu 3}$ decay events are identifiable.

The background "decays" include

(a) $K_{\pi 3}$ decays which are distinguishable from K_{e3} by T.o.F. and by the missing (π°) mass. A $K_{\pi 3}$ event misidentified as K_{e3} gives a missing mass $> m_{\pi^\circ}$, see Fig.16.

(b) $\gamma \rightarrow e^+e^-$ characterized by zero opening angle and trajectories which project back to the $\bar{p}p$ annihilation source.

(c) backscatters which have a 180° opening angle.

(d) $K_{\pi 2}$ decays, for which see the next section.

4.3 $K_{\pi 2}$ Decays

The decays $K^\circ \rightarrow \pi^+\pi^-$ are signalled by the $\pi^+\pi^-$ invariant mass, zero momentum perpendicular to the K° vector, fixed by the decay vertex, and a momentum parallel to the K° vector which is large (see Fig.10) and consistent with the value obtained from the $K^\pm\pi^\mp$ momenta.

Most $K_{\pi 2}$ events misinterpreted as πe events have a πe invariant mass which is close to the end point of the invariant mass distribution for true K_{e3} events. There are relatively few $K_{\ell 3}$ events near the end point and most of these are unidentifiable by time of flight in any case, and therefore useless.

The $K_{\pi 2}$ decays between C_4 and C_{20} are concentrated within a few cm of C_4, and those between C_{20} and C_{100} similarly close to C_{20}.

4.4 K_L Decays $> C_{20}$

The K_L decays between C_{20} and C_{100} are identified by the existence of a $K^\pm\pi^\mp$ pair and the position of the decay vertex. The $K_{e3} + K_{\mu 3} + K_{\pi 3}$ are subject to a check on the (ν or π°) missing mass and for about half the events can be identified by time of flight.

The backgrounds due to pionic annihilations, $\pi^+\pi^-e^+e^-$ and backscatters, have "decay" particles with extreme opening angle and recognizable trajectories. The decay vertices for $K_S \rightarrow \pi^+\pi^-$ are concentrated in a small fraction of the volume between C_{20} and C_{100}, and the events are readily identified by kinematics (see §4.3).

4.5 K^+K^- Events

The trigger requirements of collinearity, a fixed momentum of 800 MeV/c, and a decay between C_{20} and C_{100} are practically unambiguous as an identification of a K^+K^- pair. Of the $K^\pm$ decays 85% are two body, $\mu^+\nu$ and $\pi^+\pi^\circ$, which provides a relation between decay angle and momentum.

5. Systematic Errors

All of the measurements are concerned with fractional differences of $\sim 10^{-3}$ to 10^{-4} of count rates for charged particles of opposite charge sign. There are at least four distinct sources of spurious differences which must be considered,

(i) mechanical asymmetries
(ii) interactions of particles which depend on the sign of the charge,
(iii) backgrounds which are naturally asymmetric, or which can dilute a genuine asymmetry signal,
(iv) the $\mathbf{v} \times \mathbf{B}$ asymmetry in the drift chamber, and
(v) $\bar{p}n$ annihilations.

At the level of 10^{-4} it may not be permissible to neglect second order effects due to two of these sources of systematic error.

5.1 Mechanical asymmetries

In principle the apparatus is cylindrically symmetric and uniform. In practice there will be small mechanical asymmetries and variations of efficiency which are difficult to determine accurately; e.g. a poor scintillator strip creates a bias if the rest of the apparatus is not symmetric about the plane specified by the poor strip and the $\bar{p}p$ source. It is proposed to cancel such errors by reversing the magnetic field between LEAR beam spills and averaging the measurements. Reversing the field has, for mechanical asymmetries, the same effect as reversing the charge signs of all the particles. Any residual errors should be apparent in the differences for the pionic annihilation channels.

5.2 Interactions of Particles.

No significant errors or biasses arise from the electromagnetic interactions, ionization, multiple scattering, bremsstrahlung, and positron annihilation, and we are concerned only with the difference of the strong interactions of pairs of hadrons of opposite charge or strangeness. Furthermore for the neutral kaon decays which determine $\mathrm{Re}\,\epsilon$ and $\mathrm{Re}\,\Delta$ the decay products, $\pi^+\pi^-$ and all K_L decays, are the same independent of the initial state of the neutral kaon as K° or $\bar{K}^\circ$, and no error can be caused by the interaction of the decay particles.

Errors could arise from the differences of a few tenths of a percent for the scintillator efficiencies for (a) $K^+\pi^-$ and $K^-\pi^+$, and (b) π^+ of $\pi^+e^-\bar{\nu}$ decays and π^- of $\pi^-e^+\nu$ decays. By a factor of $\sim 10^2$ the scintillators are a more important source of error than the chambers simply because of the mass involved. It is proposed to measure the efficiencies using the annihilation

$$\bar{p}p \rightarrow K^\pm\pi^\mp K^\circ$$

and the decay $K^\circ \rightarrow \pi^+\pi^-$ inside C_{20}, with the multiplicity pattern 2, 4, 4, ≥ 2. Some 10^4 events would determine the difference of counting efficiencies with an uncertainty of $\sim 10^{-5}$ for both $K^\pm\pi^\mp$ and $\pi^\pm e^\mp\nu$, subject to minor corrections for the momentum dependence of the efficiencies. For K_{e3} decays between C_{20} and C_{100} it is proposed to use the calibration trigger (section 3.4d)

$$\bar{p}p \rightarrow K^\pm\pi^\mp K^\circ, \quad K^\circ \rightarrow \pi^+\pi^- < C_{20}, \quad K^\pm \rightarrow \pi^\pm\pi^+\pi^- > C_{20}$$

Potentially there are also errors of under 10^{-4} due to the interactions of pions and kaons in the materials surrounding the $\bar{p}p$ annihilation source and elsewhere which could cause a differential loss of good events. For pions the difference of the π^+ and π^- cross-sections for hydrogen and nuclei are known very accurately and are nearly zero for $N = Z$ nuclei, and the corrections can be calculated with confidence. The kaon cross-sections are less well known and amount to a $\bar{K}/K$ difference of $\sim$ 20mb per free nucleon (less per nucleon in nuclei), equivalent to a bias of $\sim 10^{-5}$ per mg/cm^2. However the error cancels for the small liquid hydrogen target since the kaons always come as $K\bar{K}$ pairs, $K^+\bar{K}^\circ$ or K^-K°, and for other materials it is possible to introduce a relatively thick sample between C_4 and C_{20} and measure the difference for K^+ and K^-. Beyond a few K_S decay lengths from the source the neutral kaons, K° and $\bar{K}^\circ$, both become K_L.

It is noted that the measurement of the CPT parameter $\mathrm{Re}\,\Delta$ is independent of *any* of the interaction corrections, and $\mathrm{Re}\,\Delta$ could be determined by X, equation (A19), which is the fractional difference for K° and $\bar{K}^\circ$ source particles for the K_L decays normalized to the K_S decays separately for K° and $\bar{K}^\circ$. This is a powerful check on the reliability of the corrections for $K^\pm\pi^\mp$. Similarly a remeasurement of the known[8] lepton asymmetry, δ_e and $\bar{\delta}_e$, equations (A13) and (A14), verifies the corrections for $\pi^\pm e^\mp\nu$.

5.3 Backgrounds

The only "background" which is known to be asymmetric between K° and $\bar{K}^\circ$ is the $K_{\pi 2}$ decays which represent a background to the K_{e3} and other K_L decays. For the

K_S/K_L interference terms which give $Im\Delta$ and other parameters the interesting region is in the neighbourhood of $\Gamma_S t \simeq \pi$ (see Appendix I). Integrating the decays over the range $\pi/2 \leq \Gamma_S t \leq 3\pi/2$ gives a $K^\circ/\bar{K}^\circ$ asymmetry (as defined by (A16) and (A8))

of $-1.64|\eta_{+-}|$ for $K_{\pi 2}$ decays,

and $1.30 Im\Delta$ for K_{e3} decays,

without much sensitivity to the range of integration. (Parameters in $\alpha_e(Z)$, equation (A8), other than $Im\Delta$ have been omitted for simplicity). A small contamination of K_{e3} events by $K_{\pi 2}$ events can be tolerated for the purpose of determining $Im\Delta$.

For K_L decays between C_{20} and C_{100} the $K_{\pi 2}$ background can be avoided simply by applying a cut to the fiducial volume for the decay vertices which excludes the region close to C_{20}.

The other sources of background are all symmetric with respect to K° and $\bar{K}^\circ$ and cannot create a false asymmetry.

5.4 Wire Chamber $\mathbf{v} \times \mathbf{B}$ Asymmetry

The trajectories in a magnetic field of the particles $a^+b^-c^+d^-$ of some event are identical with the trajectories of $a^-b^+c^-d^+$ of some "anti"-event in the reversed field. However the trajectories are recorded as a result of ionization electrons drifting to wires along paths which are curved due to the Lorentz force $\mathbf{v} \times \mathbf{B}$, and these curvatures change sign with the reversal of $\mathbf{B}$, thus destroying the exact equivalence of event and anti-event.

The $\mathbf{v} \times \mathbf{B}$ effect for the proportional wire chambers is insignificant. For the drift chamber of Fig.6 the drift paths are parabolic deviating by about 3mm from the radial path to an anode at a distance of 2cm for a magnetic field of 0.3 Tesla and a minimum electric field of 1 kV/cm. Even with gross mechanical asymmetries it is difficult to invent an appreciable event/anti-event bias, but it is desirable to minimize the risk by keeping the drift paths short and approximately cylindrically symmetric about the anodes. There is no readily available check on a $\mathbf{v} \times \mathbf{B}$ bias.

5.5 $\bar{p}n$ Annihilations

Some small fraction of the $\bar{p}$ beam is likely to stop in the mylar of the liquid hydrogen target and give rise to annihilations in ^{12}C,

$$\bar{p}n \to K^- K^\circ \pi^+ (\pi^-)$$
$$\text{and } \bar{p}n \to K^+ \bar{K}^\circ \pi^- (\pi^-)$$

at *unequal* rates. Such events with the (π^-) undetected would be accepted by time of flight and kinematics as good events, if the source vertex ($\sigma \simeq$ 0.5mm) is acceptable and if the nuclear debris from the ^{12}C annihilation does not trigger C_4.

Any significant fraction of $\bar{p}n$ annihilations would give rise to a gross difference between the rates for events with $\pi^+\pi^-\pi^-$ emanating from the source and those with $\pi^-\pi^+\pi^+$. If such a difference were observed it would be necessary to restrict consideration of apparent $K^\pm \pi^\mp K^\circ \pi^\circ$ annihilations to those with a π° vector within the solid angle of the detectors.

5.6 K^+K^- Systematic Errors

There are two potential sources of asymmetry between K^+ and K^- decays, viz., a difference of the efficiency of the outer detectors for K^+ and K^-, and interactions between C_{20} and C_{100} simulating a decay. Interactions inside C_{20} destroy the collinearity required for a trigger.

There is a copious supply of non-decaying K^+K^- pairs which can be used to calibrate the efficiency of the outer detectors to more than adequate accuracy.

The interactions of $K^{\pm}$ in the helium are equivalent to a fractional difference of the K^+/K^- lifetimes of a few parts in 10^4, but the decay events are accepted only if the decay angle, $\sim 30°$, and momentum, ~ 500 MeV/c, are consistent with a $\mu^{\pm}\nu$ or $\pi^{\pm}\pi^{\circ}$ decay. This requirement is expected to reduce the interaction bias to a few parts in 10^5.

6. Statistical Errors

The statistical errors are estimated for a net effective 10^{12} $\bar{p}p$ annihilations, disregarding the rate dependent losses due to dead time or inefficiency in extracting good events from the raw data tapes. For a beam of 10^6 $\bar{p}$ per second, the maximum that could be handled comfortably, a total of $\sim 2 \times 10^{12}$ $\bar{p}$ would be required to obtain the statistical accuracy given in Table IV.

Table V

Statistical Accuracy of Measured $K/\bar{K}$ Differences for 10^{12} $\bar{p}$

Annihilation	Decay	No of Events	Parameter	Stat. Error σ(Parameter)
	K_L	5×10^7	$\gamma_L = 2\,\mathrm{Re}(\epsilon + \Delta)$	1.4×10^{-4}
$K^{\pm}\pi^{\mp}K^{\circ}(n\pi^{\circ})$	$\pi^+\pi^-$	1×10^8	$D_{\pi 2} = 2\,\mathrm{Re}(\epsilon - \Delta)$	1.0×10^{-4}
	$\pi^{\pm}e^{\mp}\nu$	5×10^6	$\alpha_e, \beta_e, \gamma_{e^+}, \gamma_{e^-}$ for $\Gamma_S t \sim \pi$	$\times 10^{-4}$
K^+K^-	$\mu^{\pm}\nu + \pi^+\pi^{\circ}$	8.5×10^7	$(\tau_+ - \tau_-)/(\tau_+ + \tau_-)$	1.1×10^{-4}

The parameters represent various $K/\bar{K}$ fractional differences for the decays and are defined in Appendix I.

The proposed measurements of Table IV together with the accurately known properties[17)] of neutral kaons, *viz.* M_S, M_L, Γ_S, Γ_L, η_{+-}, η_{00} and δ_e, allow the evaluation of tests of a number of symmetry principles at a level of accuracy at which some positive results are certain. Table V lists the tests, the accuracy which could be achieved, and the present knowledge (without prejudicial assumptions, see Appendix I).

Table VI
Statistical Accuracy of the Tests of Symmetry Principles for 10^{12} $\bar{p}$

Parameter	Non-Zero for a Failure of	Experimental Sources	Stat. Error σ (Parameter)	CPT, $\Delta Q = \Delta S$ Prediction	Present Value
Re ϵ	CP and T	γ_L, $D_{\pi 2}$, η_{+-}	0.5×10^{-4}	16×10^{-4}	$< 4 \times 10^{-2}$
Imϵ	CP and T	K_{e3}, δ_e, η_{+-}, η_{00}	6×10^{-4}	16×10^{-4}	—
Re Δ	CP and CPT	γ_L, $D_{\pi 2}$, η_{+-}	0.5×10^{-4}	0	$< 3 \times 10^{-2}$
ImΔ	CP and CPT	K_{e3}, δ_e	6×10^{-4}	0	—
$\frac{(M-\bar{M})}{(M_L-M_S)}$	CP and CPT	Re & ImΔ	6×10^{-4}		—
$\frac{(\Gamma-\bar{\Gamma})}{(\Gamma_S-\Gamma_L)}$			* (1×10^{-4})	0	*$(< 3 \times 10^{-2})$
Re y_e	CP and CPT in K_{e3}	$D_{\pi 2}$, η_{+-}, δ_e	2×10^{-4}	0	$< 3 \times 10^{-2}$
$\beta_e(\infty)$	T	K_{e3}, $D_{\pi 2}$, η_{+-}, δ_e	4×10^{-4}	65×10^{-4}	—
$\frac{(\Gamma^+-\Gamma^-)}{(\Gamma^++\Gamma^-)}$	CP and CPT	K^+K^-	1×10^{-4}	0	$< 15 \times 10^{-4}$
Unitarity	Hermiticity	All K°	0.1%	0	—
$\frac{1}{2}\mathrm{Im}(x_e + \bar{x}_e)$	$\Delta Q = \Delta S$	K_{e3}, γ_L, δ_e	8×10^{-4}	0	$(-4 \pm 26) \times 10^{-3}$

* assuming unitarity

In essence the $K^\circ/\bar{K}^\circ$ difference for $\pi^+\pi^-$ decays, $D_{\pi 2}$, determines the state of CP/CPT invariance in K_{e3} decays, $\mathrm{Re}(y_e + x_e - \bar{x}_e)$, and permits the direct demonstration of a failure of time reversal invariance. This is the argument set out in Fig.2 which is expected to exhibit a failure of time reversal invariance of 6.5×10^{-3} with statistical error of 0.4×10^{-3}.

7.1 Beam Request

The design magnitude for the tests of symmetry principles is 10^{12} antiprotons at a rate not exceeding $10^6 \bar{p}\,\mathrm{s}^{-1}$. It would not be very profitable to use a more intense beam as the wire chamber readout is limited to $10MH_Z$, and there is a considerable risk of creating biasses indirectly as a result of complicated events with many stray hits. Generally it would be much preferred to take data at a $\bar{p}$ rate somewhat below $10^6\,\mathrm{s}^{-1}$.

The statistical accuracy provided by $10^{12}\bar{p}$, Tables V and VI, is not exhaustive in the sense that the statistical errors are very small compared with the expected systematic errors, but the accuracy is sufficient to reach a confident conclusion if the orthodox assumption of CPT invariance and T violation prevails.

It is planned to run the various tests in parallel together with the calibrations required. This is certainly possible for all the $K^\circ/\bar{K}^\circ$ comparisons but the technical requirements for the simultaneous recording of the K^+/K^- comparison have not yet been fully developed.

7.2 Time Table

The Jade magnet is expected to become available towards the end of 1986 and it is estimated that it will require approximately the calendar year of 1987 to dismantle, repair, modify, ship, and install the magnet and power supply. The year 1987 conveniently coincides with the Acol shut-down. A further year, 1988, will be required to install, and cable the counting equipment in the magnet. Apart from tests no beam would be requested before 1989.

Appendix I.

Theoretical Summary.[16.]

For present purposes it is sufficient to define two orthogonal eigen states of the strong interaction, $|K^\circ>$ and $|\bar{K}^\circ>$, and to assume that the time development of an arbitrary state

$$|\psi>= a|K^\circ> +\bar{a}|\bar{K}^\circ> \tag{A1}$$

is given by

$$-\frac{d}{dt}\binom{a}{\bar{a}} = (i\mathbf{M} + \frac{1}{2}\mathbf{\Gamma})\binom{a}{\bar{a}} \tag{A2}$$

where $\mathbf{M}$ and $\mathbf{\Gamma}$ are 2×2 matrices and can be chosen to be hermitian without loss of generality. The matrix $(i\mathbf{M} + \frac{1}{2}\mathbf{\Gamma})$ contains 8 real numbers, all of which can be determined experimentally without assumptions concerning CP, T, and CPT invariance or hermiticity.

Diagonalizing $(i\mathbf{M} + \frac{1}{2}\mathbf{\Gamma})$ gives the eigen vectors $|K_S>$ and $|K_L>$ with eigen values $(iM_S + \frac{1}{2}\Gamma_S)$ and $(iM_L + \frac{1}{2}\Gamma_L)$.

$$\sqrt{2}\mid K_S>= (1+\epsilon+\Delta)|K^\circ> +(1-\epsilon-\Delta)|\bar{K}^\circ> \tag{A3}$$

$$\sqrt{2}\mid K_L>= (1+\epsilon-\Delta)|K^\circ> -(1-\epsilon+\Delta)|\bar{K}^\circ>$$

where

$$\epsilon = \{-\mathrm{Im}\mathrm{M}_{12} + \frac{\mathrm{i}}{2}\mathrm{Im}\Gamma_{12}\}/\{\mathrm{i}(\mathrm{M_S} - \mathrm{M_L}) + \frac{1}{2}(\Gamma_\mathrm{S} - \Gamma_\mathrm{L})\} \tag{A4}$$

$$\Delta = \{i(M_{11} - M_{22}) + \frac{1}{2}(\Gamma_{11} - \Gamma_{22})\}/\{2i(M_S - M_L) \ + \ (\Gamma_S - \Gamma_L)\}$$

and the eigen values for $|K_S>$ and $|K_L>$ are

$$\frac{i}{2}(M_{11} + M_{22}) + \frac{1}{4}(\Gamma_{11} + \Gamma_{22}) \pm (-i\,\mathrm{Re}\,M_{12} + \frac{1}{2}\,\mathrm{Re}\,\Gamma_{12}) \tag{A5}$$

Small terms quadratic in ϵ and Δ have been neglected here and later.

CP	invariance requires	$\epsilon = \Delta = 0$
CPT	invariance requires	$\Delta = 0$
T	invariance requires	$\epsilon = 0$

Of the eight real numbers required to specify $(i\mathbf{M}+\frac{1}{2}\mathbf{\Gamma})$ four are provided by the masses and decay rates of K_S and K_L. One is necessarily arbitrary since the relative phase of $|K^\circ>$ and $|\bar{K}^\circ>$ cannot be determined by the strong interaction, and usually this is chosen such that

$$\mathrm{Im}(\epsilon - \Delta) = \mathrm{Im}(2\eta_{+-} + \eta_{\circ\circ})/3 \tag{A6}$$

where η_{+-} and $\eta_{\circ\circ}$ are the ratios of amplitudes of the K_L and K_S decays to $\pi^+\pi^-$ and $\pi^\circ\pi^\circ$. The three remaining numbers could be $\mathrm{Re}\,\epsilon$, $\mathrm{Re}\,\Delta$ and $\mathrm{Im}\Delta$.

As CPT invariance is *not* assumed it is necessary to consider the possibility of a direct CP violation in $K_{\ell 3}$ decays[5)] *i.e.* a difference of the $\pi\ell\nu$ partial width for K° and the anti $(\pi\ell\nu)$ partial width for $\bar{K}^\circ$. In principle this could occur either in the $\Delta Q = \Delta S$ amplitude, fractional difference y_ℓ, or in the $\Delta Q = -\Delta S$ amplitude, fractional difference $x_\ell - \bar{x}_\ell$ relative to $\Delta Q = \Delta S$. Since these additional parameters satisfy T invariance they invalidate the direct demonstration of a failure of T invariance advocated in reference[4]. Our only knowledge of this possible new CP failure comes from the lepton asymmetry[8] δ_ℓ which indicates that, if this CP failure exists, it is the same for μ and e,

$$\delta_\mu(\infty) - \delta_e(\infty) = \mathrm{Re}(y_e + x_e - \bar{x}_e) - \mathrm{Re}(y_\mu + x_\mu - \bar{x}_\mu) = (0.28 \pm 0.34) \times 10^{-3} \quad (A7)$$

c.f. the average $\delta_\ell = (3.30 \pm 0.12) \times 10^{-3}$.

For simplicity the formulae for the fractional differences between decays of neutral kaons initially K° or $\bar{K}^\circ$ are given in terms of a parameter $Z \simeq (M_L - M_S)t \simeq \frac{1}{2}\Gamma_S t \simeq \frac{1}{2}(\Gamma_S - \Gamma_L)t$. Rates for decay to a channel i are written R_i for an initial K° and $\bar{R}_i$ for an initial $\bar{K}^\circ$.

i:	$\pi 2$	$\pi 3$	e^+	e^-	μ^+	μ^-
Decay:	$\pi^+\pi^-$	$\pi^+\pi^-\pi^\circ$	$\pi^- e^+ \nu$	$\pi^+ e^- \bar{\nu}$	$\pi^- \mu^+ \nu$	$\pi^+ \mu^- \bar{\nu}$

with $\ell^\pm = e^\pm$ or $\mu^\pm$, and $L = e^+ + e^- + \mu^+ + \mu^- + \pi 3$.

An integral sign is used to indicate a sum of all events in the region of K_S decays, which integral can be evaluated but depends in a complicated way on the momentum distribution of the kaons and the dimensions of the experimental apparatus. The expressions for $Z = \infty$ are the asymptotic values in the K_L regions. Apart from the $\pi^+\pi^-$ decay asymptotia exists for $Z > \pi$, $\Gamma_S t \gtrsim 2\pi$.

It is convenient to define the following measurable differences,

$$\begin{aligned}
\alpha_\ell(Z) &= (\bar{R}_{\ell^-} - R_{\ell^+})/(\bar{R}_{\ell^-} + R_{\ell^+}) \\
&= \mathrm{Re}\, y_\ell + \frac{\mathrm{Re}(4\Delta + x_\ell - \bar{x}_\ell)\sinh Z + \mathrm{Im}(4\Delta + x_\ell + \bar{x}_\ell)\sin Z}{\cosh Z + \cos Z} \qquad (A8) \\
\alpha_\ell(\infty) &= 4\,\mathrm{Re}\,\Delta + \mathrm{Re}(y_\ell + x_\ell - \bar{x}_\ell) = \gamma_L - \delta_\ell(\infty)
\end{aligned}$$

$$\begin{aligned}
\beta_\ell(Z) &= (\bar{R}_{\ell^+} - R_{\ell^-})/(\bar{R}_{\ell^+} + R_{\ell^-}) \\
&= \mathrm{Re}(4\epsilon - y_\ell) + \frac{\mathrm{Re}(\bar{x}_\ell - x_\ell)\sinh Z + \mathrm{Im}(x_\ell + \bar{x}_\ell)\sin Z}{\cosh Z - \cos Z} \qquad (A9) \\
&\simeq \{\mathrm{Im}(x_\ell + \bar{x}_\ell) - \mathrm{Re}(x_\ell - \bar{x}_\ell)\}/Z, \quad \text{for} \quad |x_\ell|, |\bar{x}_\ell| \ll Z \ll 1 \\
\beta_\ell(\infty) &= 4\,\mathrm{Re}\,\epsilon - \mathrm{Re}(y_\ell + x_\ell - \bar{x}_\ell) = \gamma_L + \delta_\ell(\infty)
\end{aligned}$$

$$\begin{aligned}
\gamma_\ell(Z) &= (\bar{R}_\ell - R_\ell)/(\bar{R}_\ell + R_\ell), \quad \ell = \ell^+ + \ell^- \\
&= 2\,\mathrm{Re}\,\epsilon + 2\,\mathrm{Re}\,\Delta \tanh Z + \frac{\mathrm{Re}(y_\ell - 2\epsilon)\cos Z + \mathrm{Im}(2\Delta + x_\ell - \bar{x}_\ell)\sin Z}{\cosh Z} \qquad (A10) \\
\gamma_\ell(\infty) &= 2\,\mathrm{Re}(\epsilon + \Delta) = \gamma_{\ell^+}(\infty) = \gamma_{\ell^-}(\infty) = \gamma_L \\
\gamma_{\ell^+}(Z) &= 2\,\mathrm{Re}\,\epsilon + 2\,\mathrm{Re}\,\Delta \tanh Z + \frac{(-1 - 2\,\mathrm{Re}\,\epsilon)\cos Z + \mathrm{Im}(2\Delta + 2x_\ell)\sin Z}{\cosh Z} \qquad (A11) \\
\gamma_{\ell^-}(Z) &= 2\,\mathrm{Re}\,\epsilon + 2\,\mathrm{Re}\,\Delta \tanh Z \\
&\quad + \frac{[1 - \mathrm{Re}(2\epsilon - 2y_\ell)]\cos Z + \mathrm{Im}(2\Delta + 2\bar{x}_\ell)\sin Z}{\cosh Z} \qquad (A12)
\end{aligned}$$

$$\begin{aligned}\delta_\ell &= (R_{\ell+} - R_{\ell-})/(R_{\ell+} + R_{\ell-})\\ &= \mathrm{Re}(2\epsilon - y_e) - \mathrm{Re}(2\Delta + x_\ell - \bar{x}_\ell)\tanh Z\\ &+ \frac{(1-\mathrm{Re}(2\epsilon - y_\ell))\cos Z - \mathrm{Im}(2\Delta - \mathrm{x}_\ell + \bar{\mathrm{x}}_\ell)\sin \mathrm{Z}}{\cosh \mathrm{Z}}\end{aligned} \qquad (A13)$$

$$\begin{aligned}\bar{\delta}_\ell(Z) &= (\bar{R}_{\ell+} - \bar{R}_{\ell-})/(\bar{R}_{\ell+} + \bar{R}_{\ell-})\\ &= \mathrm{Re}(2\epsilon - y_\ell) - \mathrm{Re}(2\Delta + x_\ell - \bar{x}_\ell)\tanh Z\\ &+ \frac{-(1+\mathrm{Re}(2\epsilon + y_\ell))\cos Z - \mathrm{Im}(2\Delta - \mathrm{x}_\ell + \bar{\mathrm{x}}_\ell)\sin \mathrm{Z}}{\cosh \mathrm{Z}}\end{aligned} \qquad (A14)$$

$$\delta_\ell(\infty) = \bar{\delta}_\ell(\infty) = 2\,\mathrm{Re}(\epsilon - \Delta) - \mathrm{Re}(y_\ell + x_\ell - \bar{x}_\ell)$$

$$\begin{aligned}\gamma_{\pi 3}(Z) &= (\bar{R}_{\pi 3} - R_{\pi 3})/(\bar{R}_{\pi 3} + R_{\pi 3})\\ &= 2\,\mathrm{Re}(\epsilon + \Delta) - 2e^{-Z}|\eta_{+-\mathrm{o}}|\cos(Z + \phi_{+-\mathrm{o}})\\ \gamma_{\pi 3}(\infty) &= 2\,\mathrm{Re}(\epsilon + \Delta) = \gamma_L\end{aligned} \qquad (A15)$$

$$\begin{aligned}\gamma_{\pi 2}(Z) &= (\bar{R}_{\pi 2} - R_{\pi 2})/(\bar{R}_{\pi 2} + R_{\pi 2})\\ &= \{2\,\mathrm{Re}(\epsilon - \Delta) - 2e^{Z}|\eta_{+-}|\cos(Z - \phi_{+-})\}/(1 + |\eta_{+-}|^2 e^{2Z})\\ \gamma_{\pi 2}(0) &= 2\,\mathrm{Re}(\epsilon - \Delta - \eta_{+-})\end{aligned} \qquad (A16)$$

$$\begin{aligned}\gamma_L(\infty) &= (\bar{R}_L - R_L)/(\bar{R}_L + R_L)\\ &= 2\,\mathrm{Re}(\epsilon + \Delta)\end{aligned} \qquad (A17)$$

$$\begin{aligned}D_{\pi 2} &= \left(\int \bar{R}_{\pi 2} - \int R_{\pi 2}\right) \Big/ \left(\int \bar{R}_{\pi 2} + \int R_{\pi 2}\right)\\ &= 2\,\mathrm{Re}(\epsilon - \Delta) + f(\eta_{+-})\end{aligned} \qquad (A18)$$

$$\begin{aligned}X &= \left(\bar{R}_L/\int \bar{R}_{\pi 2} - R_L/\int R_{\pi 2}\right) \Big/ \left(\bar{R}_L/\int R_{\pi 2} + R_L/\int R_{\pi 2}\right)\\ &= 4\,\mathrm{Re}\,\Delta - f(\eta_{+-}),\ \text{for } R_L \text{ and } \bar{R}_L \text{ measured at large } Z.\end{aligned} \qquad (A19)$$

The integrated $\pi^+\pi^-$ interference term $f(\eta_{+-})$ depends on the range of integration and the value of η_{+-}, but can be calculated from the present measurements of $|\eta_{+-}|$ and ϕ_{+-} with an error of $\pm 0.1 \times 10^{-3}$.

Of these various difference measurements only $\delta_\ell(Z)$, equ. (A12) has been determined with good accuracy, but all would be accessible with a good $\bar{p}p$ annihilation source. Apart from $\delta_l(Z)$ the most interesting are the integral measurements $\gamma_L(\infty)$, eqn. (A17), and $D_{\pi 2}$ eqn. (A18) which together determine $\mathrm{Re}\,\epsilon$ and $\mathrm{Re}\,\Delta$, and the leptonic decays in the region of K_S/K_L interference at small Z. Numerically we have

$$\alpha_\ell\left(\frac{\pi}{2}\right) \simeq \alpha_\ell(\infty) + 1.6\mathrm{Im}\Delta + 0.4\mathrm{Im}(\mathrm{x}_\ell + \bar{\mathrm{x}}_\ell) \qquad (A8a)$$

$$\beta_\ell\left(\frac{1}{2}\right) \simeq \beta_\ell(\infty) + 2\mathrm{Im}(\mathrm{x}_\ell + \bar{\mathrm{x}}_\ell) - \mathrm{Re}(\mathrm{x}_\ell - \bar{\mathrm{x}}_\ell) \qquad (A9a)$$

$$\beta_\ell\left(\frac{\pi}{2}\right) \simeq \beta_\ell(\infty) + 0.4\mathrm{Im}(\mathrm{x}_\ell + \bar{\mathrm{x}}_\ell) \qquad (A9b)$$

$$\gamma_\ell\left(\frac{\pi}{2}\right) \simeq \gamma_\ell(\infty) + 0.8\mathrm{Im}\Delta + 0.4\mathrm{Im}(\mathrm{x}_\ell + \bar{\mathrm{x}}_\ell) \qquad (A10a)$$

$$\gamma_{\ell+}\left(\frac{\pi}{2}\right) \simeq \gamma_\ell\left(\frac{\pi}{2}\right) + 0.4\mathrm{Im}\mathrm{x}_\ell \qquad (A11a)$$

$$\gamma_{\ell-}\left(\frac{\pi}{2}\right) \simeq \gamma_\ell\left(\frac{\pi}{2}\right) + 0.4\mathrm{Im}\bar{\mathrm{x}}_\ell \qquad (A12a)$$

which together with $\gamma_L(\infty)$, $D_{\pi 2}$, and the known $\delta_\ell(\infty)$ can determine

$$\mathrm{Re}\,\epsilon, \mathrm{Re}\,\Delta, \mathrm{Im}\Delta, \mathrm{Re}\,\mathrm{y}_\ell, \mathrm{Re}(\mathrm{x}_\ell - \bar{\mathrm{x}}_\ell), \mathrm{Im}\mathrm{x}_\ell, \text{and } \mathrm{Im}\bar{\mathrm{x}}_\ell$$

and $\mathrm{Im}\epsilon$ is determined by the phase convention, equ. (A6), *i.e.* all the parameters of the theory. Experimentally this translates into a requirement for the measurement of

(a) K_L decays, *i.e.* $\pi e\nu$, $\pi\mu\nu$ and $\pi\pi\pi$ collectively, for $\Gamma_S t \gtrsim 2\pi$

and

(b) $K_{\pi 2}$ and $K_{\ell 3}$ decays for $1 \lesssim \Gamma_S t \lesssim 2\pi$ under such circumstances that K° and $\bar{K}^\circ$ can be compared, thus testing

CP and T invariance in K° decays, ϵ

$R(K^\circ \to \bar{K}^\circ) \neq R(\bar{K}^\circ \to K^\circ)$ detailed balance[4]

CP and CPT invariance in K° decays, Δ

$$\begin{aligned}\mathrm{Im}\Delta - \mathrm{Re}\,\Delta &\simeq (M - \bar{M})/2(M_L - M_S)\\ \mathrm{Im}\Delta + \mathrm{Re}\,\Delta &\simeq (\Gamma - \bar{\Gamma})/2(\Gamma_S - \Gamma_L)\end{aligned} \qquad (A20)$$

CP and CPT invariance in $K_{\ell 3}$ decays, $\mathrm{Re}\,y_\ell$

$\Delta Q = -\Delta S$ in $K_{\ell 3}$ decays, $\mathrm{Im}\mathrm{x}_\ell$ and $\mathrm{Im}\bar{\mathrm{x}}_\ell$

$\Delta Q = -\Delta S$, CP and CPT invariance in $K_{\ell 3}$ decays, $\mathrm{Re}(x_\ell - \bar{x}_\ell)$

Orthodox wisdom holds that $\epsilon \neq 0$ and that all other parameters are zero, but nothing is known unless further assumptions, CPT invariance or at least hermiticity, are made.

The same measurements can also test the validity of the unitarity relation of Bell and Steinberger[11] which gives[16]

$$\begin{aligned}&(\mathrm{Re}\,\epsilon - i\mathrm{Im}\Delta)\{\mathrm{i}(\mathrm{M_L} - \mathrm{M_S}) + \frac{1}{2}(\Gamma_\mathrm{S} - \Gamma_\mathrm{L})\}\\ &= \eta_{+-}\Gamma_S(\pi^+\pi^-) + \eta_{\circ\circ}\Gamma_S(\pi^\circ\pi^\circ)\\ &+ \eta^*_{+-\circ}\Gamma_L(\pi^+\pi^-\pi^\circ) + \eta^*_{\circ\circ\circ}\Gamma_L(\pi^\circ\pi^\circ\pi^\circ)\\ &+ (\delta_e + 2\Delta^* + x^*_e - \bar{x}_e)\Gamma_L(\pi e\nu) + (\delta_\mu + 2\Delta^* + x^*_\mu)\Gamma_L(\pi_\mu\nu)\end{aligned} \qquad (A14)$$

allowing for the possible CP and CPT violation in $K_{\ell 3}$ decays. It is noted that the present best measurement[17] of the phase of $\eta_{\circ\circ}$ differs from $\tan^{-1} 2(M_L - M_S)/(\Gamma_S - \Gamma_L)$ by two stand deviations which, if confirmed, would indicate a failure of the unitarity relation (A14), or $\mathrm{Im}\Delta \neq 0$ and a failure of CPT invariance. The test of the unitarity relation would in any case be limited to about 0.1% by the uncertainty of the value of $\eta_{\circ\circ\circ}$.

Finally it should be remarked that the test of CPT invariance provided by the comparison of K^+ and K^- lifetimes has no obvious connection with the CPT test provided by the difference of decay rates, $\Gamma - \bar{\Gamma}$, of K° and $\bar{K}^\circ$, eqn. (A20).

References

1. R.H.Dalitz, *Acta Physica Austriaca,* **Suppl. XXIV**, p.393, 1982.
   J.W.Cronin, *Acta Physica Palonica,* **B15**, 419 and 721, 1984.
2. N.F.Ramsay, *Rep. Progr. Phys.* **45**, 95, 1982.
3. M.K.Campbell *et al*, *Phys. Rev.* **47**, 1032, 1982.
4. P.K.Kabir, *Phys. Rev.* **D2**, 540, 1970.
5. T.D.Lee, "Particle Physics and Introduction to Field Theory", p.366, Harwood, 1981.
6. G.Burgun *et al*, *Nucl. Phys.* **B50**, 194, 1972
   B.R.Weber *et al*, *Phys. Rev.* **D3**, 64, 1971
   Y.Cho *et al*, *Phys. Rev.* **D1**, 3031, 1970
   W.A.Mann *et al*, *Phys. Rev.* **D6**, 137, 1972.
7. R.Armenteros *et al*, *Phys. Lett.* **17**, 170, 1965
   C.Baltay *et al*, *Phys. Rev. Lett.* **15**, 591, 1965
   L.Dobrzynski *et al*, *Phys. Lett.* **22**, 105, 1966
8. G.Gewinger *et al*, *Phys. Lett.* **48B**, 483, 1974.
9. L.Fonda and G.C.Ghirardi, "Symmetry Principles in Quantum Physics", Dekker, 1970.
10. L.Wolfenstein, *Nuovo Cimento* **63**, 269, 1969.
11. J.S.Bell and J.Steinberger in Proc. Oxford Int. Conf. on Elementary Particles (Ed. Moorhouse *et al*) p.195, 1965.
12. M.Baldo-Ceolin *et al*, *JETP Lett.* **38**, 557, 1983.
13. F.Lobkowicz *et al*, *Phys. Rev.* **185**, 1676, 1969.
14. R.Armenteros and B.French in "High Energy Physics" Vol. **4**, p.237, Editor E.H.S.Burhop, Academic Press 1969.
15. J.Roehrig *et al*, *NIM* **226**, 319, 1984.
16. N.W.Tanner and R.H.Dalitz, to be published.
17. Reviews of Particle Properties, *R.M.P.* **56**, No.2, Part II, 1984.
18. The limit on the K°, $\bar{K}^\circ$ mass difference given in reference[17] has been derived *assuming* CPT invariance in the K_{e3} decays. See Cronin[1] and in particular the Addendum p.721, and also ref.[16].

Figure Captions

1. The decay rates for K° and $\bar{K}^\circ$ to $\pi^+\pi^-$ as a function of the proper time t. The difference between the curves is the physical manifestation of the failure of CP invariance.
2. The chain of reactions and decays which relates a difference of the rates for K^-e^- and K^+e^+ events to a test of detailed balance, $K^\circ \to \bar{K}^\circ$ v. $\bar{K}^\circ \to K^\circ$, and therefore a test of time reversal invariance. It is a valid test of T if there is no direct violation of CP and CPT invariance in K_{e3} decays.
3. The dependence on the proper time t of the K_{e3} difference $\alpha_e(t)$ which determines ImΔ,
$$\alpha_e(t) = (\bar{R}_{e-} - R_{e+})/(\bar{R}_{e-} + R_{e+}) \qquad (A8)$$
where $\bar{R}_{e-}$ is the rate for an initial $\bar{K}^\circ$ decaying to $\pi^+e^-\bar{\nu}$.
4. The fractional difference of the decay rates for an initial K° decaying to $\pi^+e^-\bar{\nu}$ and an initial $\bar{K}^\circ$ decaying to $\pi^-e^+\nu$ as a function of proper time i.e. the K^+e^+/K^-e^- difference of the reaction chains of Fig.2. Here the curve is drawn assuming CPT invariance and a $\Delta Q = -\Delta S$ amplitude one tenth of the present experimental limit.
5. A longitudinal section of the Jade magnet with the proposed chambers, hodoscope and beam superimposed. The length of the outer detectors is 3m.
6. A cross-section of the apparatus showing the target, the multi-wire proportional chambers C_4, C_{20} C_{100} and C_{170}, the drift chamber, and the scintillation hodoscope.
7. The detail of the central region showing the target assembly, the beam scintillator, and the proportional chambers C_4 and C_{20}.
8. Schematic diagram for the multiplicity trigger.
"CMU = Combination and Multiplicity Unit, PLU = Programmable Logic Unit"
9. The organization of the data acquisition system.
10. The K° momentum distribution for accepted $\bar{p}p \to K^\pm\pi^\mp K^\circ(n\pi^\circ)$ annihilation events for which the K° decays
(a) as K_L
(b) as K_S between C_4 and C_{20}
(c) as K_S outside C_{20}
The spectra are not normalized.
11. The distributions for (a) $K^\pm$ momentum and (b) $K^\pm$ transverse momentum, for accepted events due to $\bar{p}p \to K^\pm\pi^\mp K^\circ(n\pi^\circ)$ and K° decaying as K_L, and (c) $\pi^\pm$ momentum for the background $\bar{p}p \to \pi^+\pi^-$ etc. which gives rise to $\pi^+\pi^-e^+e^-$ and backscatter triggers.

12(a) The probability distribution for the time of flight difference Δt of kaons and pions with the same trajectory. The abscissa $\Delta t = (t_K - t_\pi)$.

(b) The time of flight error due to a $K^+\pi^-$ event being falsely identified as a $K^-\pi^+$ event. The abscissa is
$$(t_{K^-} - t_{\pi^+})_{\text{observed}} - (t_{K^-} - t_{\pi^+})_{\text{calculated}}$$
where the calculated times are determined by the measured transverse momenta and trajectories, and the masses falsely assigned.
These T.o.F. distributions correspond to the momentum distribution of Fig.11(a) i.e. all accepted events due to $\bar{p}p \to K^\pm\pi^\mp K^\circ(n\pi^\circ)$ and a K_L decay.

13. The spectrum of $K^{\pm}\pi^{\mp}$ missing mass expected for events due to $\bar{p}p \rightarrow K^{\pm}\pi^{\mp}\pi^{\circ}$ and a K_L decay.
14. The $e^{\pm}$ momentum distribution for accepted events due to $\bar{p}p \rightarrow K^{\pm}\pi^{\mp}K^{\circ}(n\pi^{\circ})$ and a K_{e3} decay.

15(a) The probability distribution for an electron from a K_{e3} decay within C_{20} having a time of flight differing from that for a pion of the same momentum and trajectory greater than $\Delta t = t_\pi - t_e$. All annihilations $K^{\pm}\pi^{\mp}K^{\circ}(n\pi^{\circ})$ are included. The time distribution is derived from the momentum distribution of Fig.14.

(b) The time difference distribution for decays to $\pi^+e^-\bar{\nu}$ within C_{20} falsely interpreted as $\pi^-e^+\nu$. The abscissa is

$$(t_{\pi^-} - t_{e^+})_{\text{observed}} - (t_{\pi^-} - t_{e^+})_{\text{calculated}}$$

where the calculated times of flight are determined by the measured momenta and the masses falsely assigned. All annihilations $K^{\pm}\pi^{\mp}K^{\circ}(n\pi^{\circ})$ are included.

16. The missing mass distribution for $K^{\circ} \rightarrow \pi^+\pi^-\pi^{\circ}$ decays correctly identified and falsely identified as $\pi e\nu$.

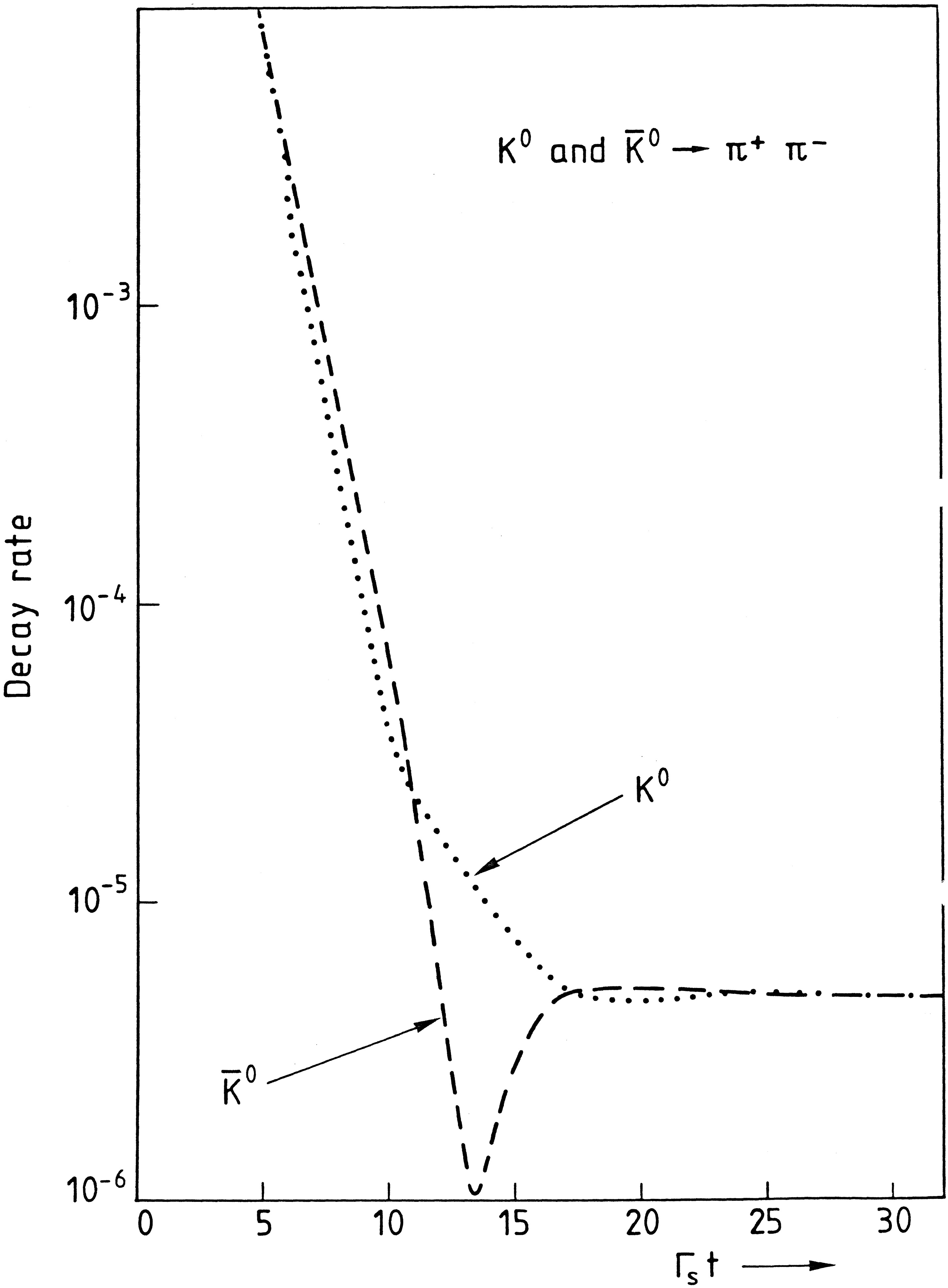

K^0 and $\bar{K}^0 \rightarrow \pi^+ \pi^-$
K^0
$\bar{K}^0$
Decay rate
10^{-3}
10^{-4}
10^{-5}
10^{-6}
0
5
10
15
20
25
30
$\Gamma_s t$

Fig. 1

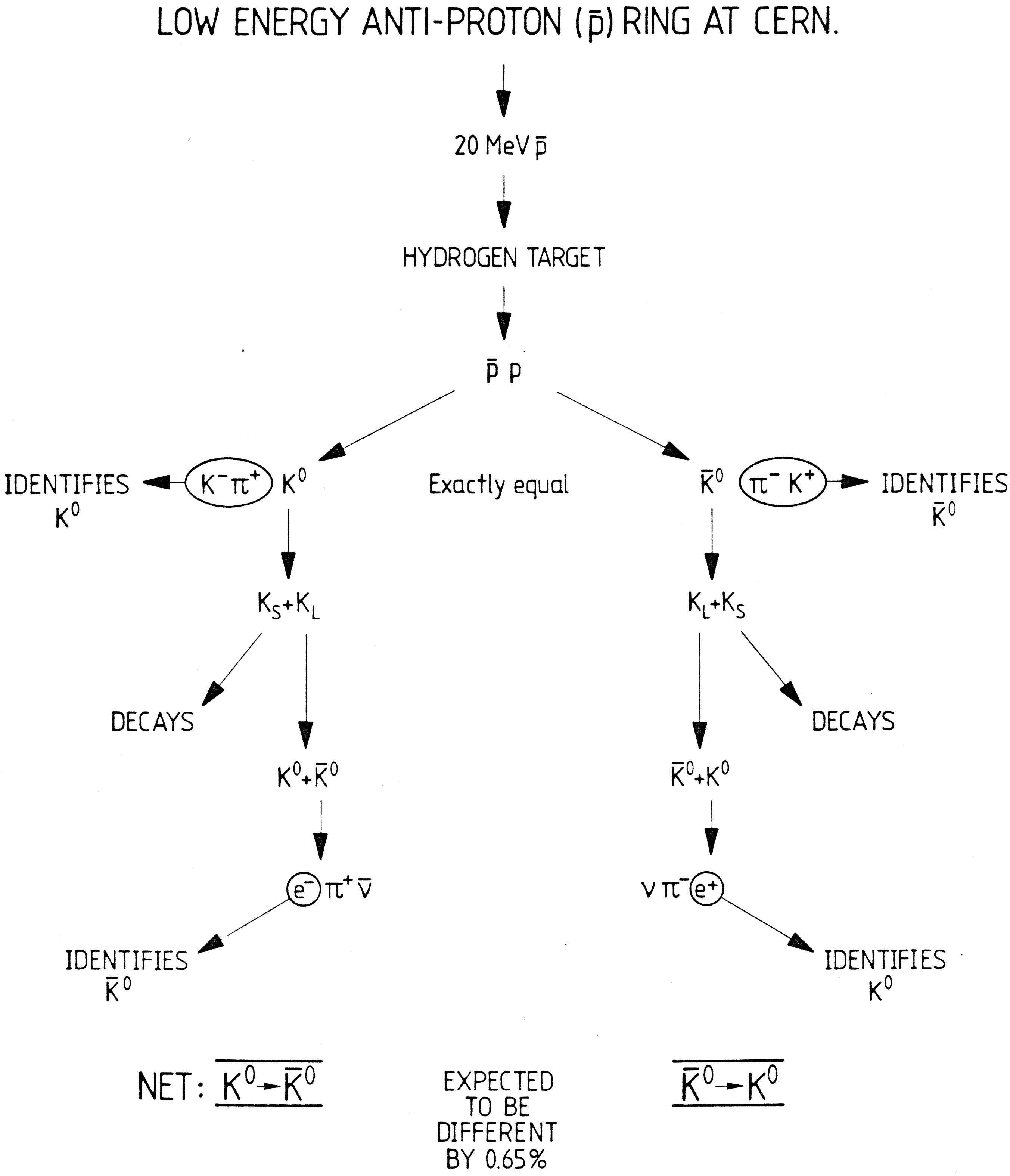
LOW ENERGY ANTI-PROTON ($\bar{p}$) RING AT CERN.
20 MeV $\bar{p}$
HYDROGEN TARGET
$\bar{p}$ p
IDENTIFIES K^0
$K^- \pi^+$
K^0
Exactly equal
$\bar{K}^0$
$\pi^- K^+$
IDENTIFIES $\bar{K}^0$
$K_S + K_L$
$K_L + K_S$
DECAYS
DECAYS
$K^0 + \bar{K}^0$
$\bar{K}^0 + K^0$
$e^- \pi^+ \bar{\nu}$
$\nu \pi^- e^+$
IDENTIFIES $\bar{K}^0$
IDENTIFIES K^0
NET: $\overline{\underline{K^0 \to \bar{K}^0}}$
EXPECTED TO BE DIFFERENT BY 0.65%
$\overline{\underline{\bar{K}^0 \to K^0}}$

Fig. 2

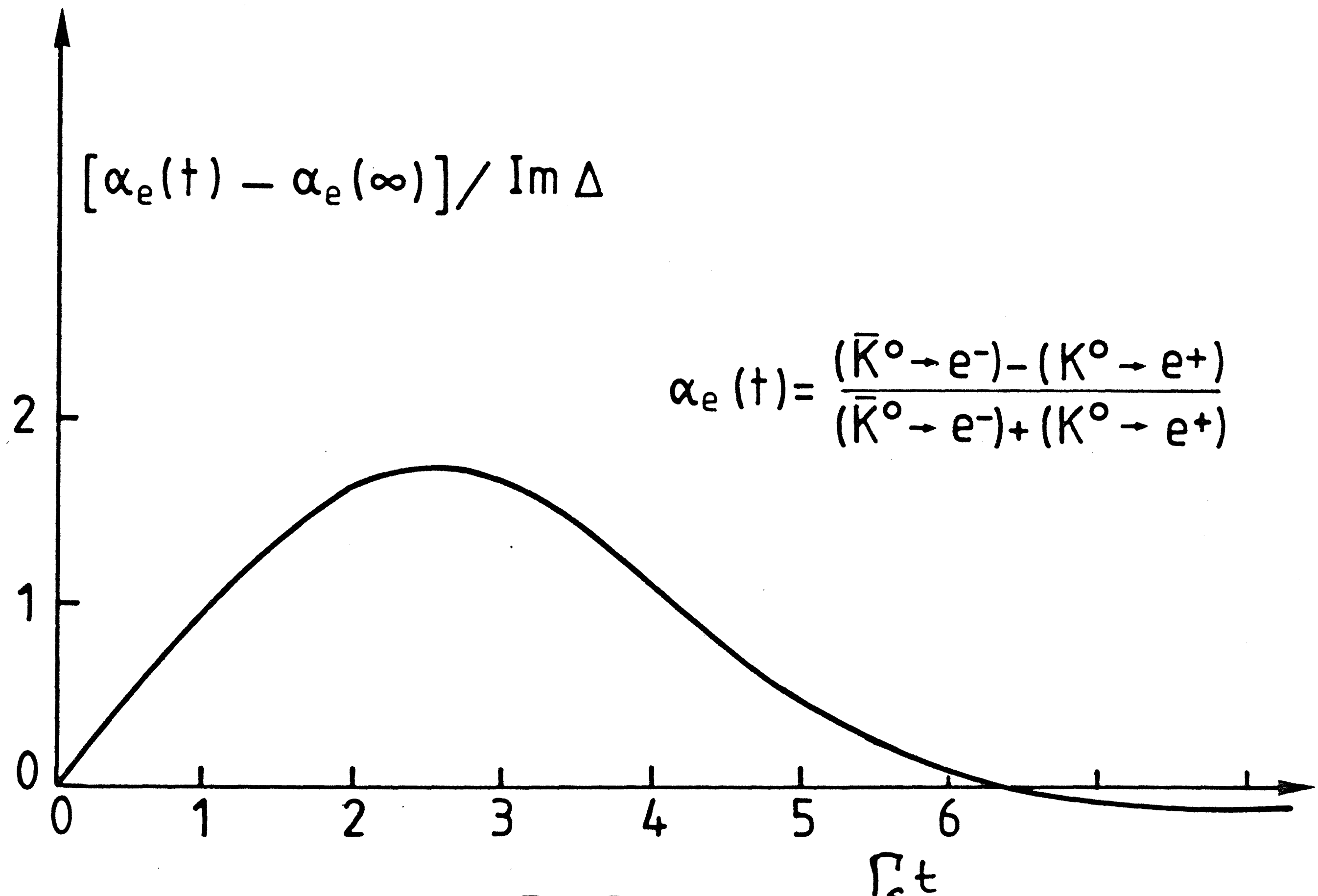

$[\alpha_e(t) - \alpha_e(\infty)]/\,\mathrm{Im}\,\Delta$
$\alpha_e(t) = \frac{(\bar{K}^0 \to e^-) - (K^0 \to e^+)}{(\bar{K}^0 \to e^-) + (K^0 \to e^+)}$
2
1
0
0
1
2
3
4
5
6
$\Gamma_s t$

Fig. 3

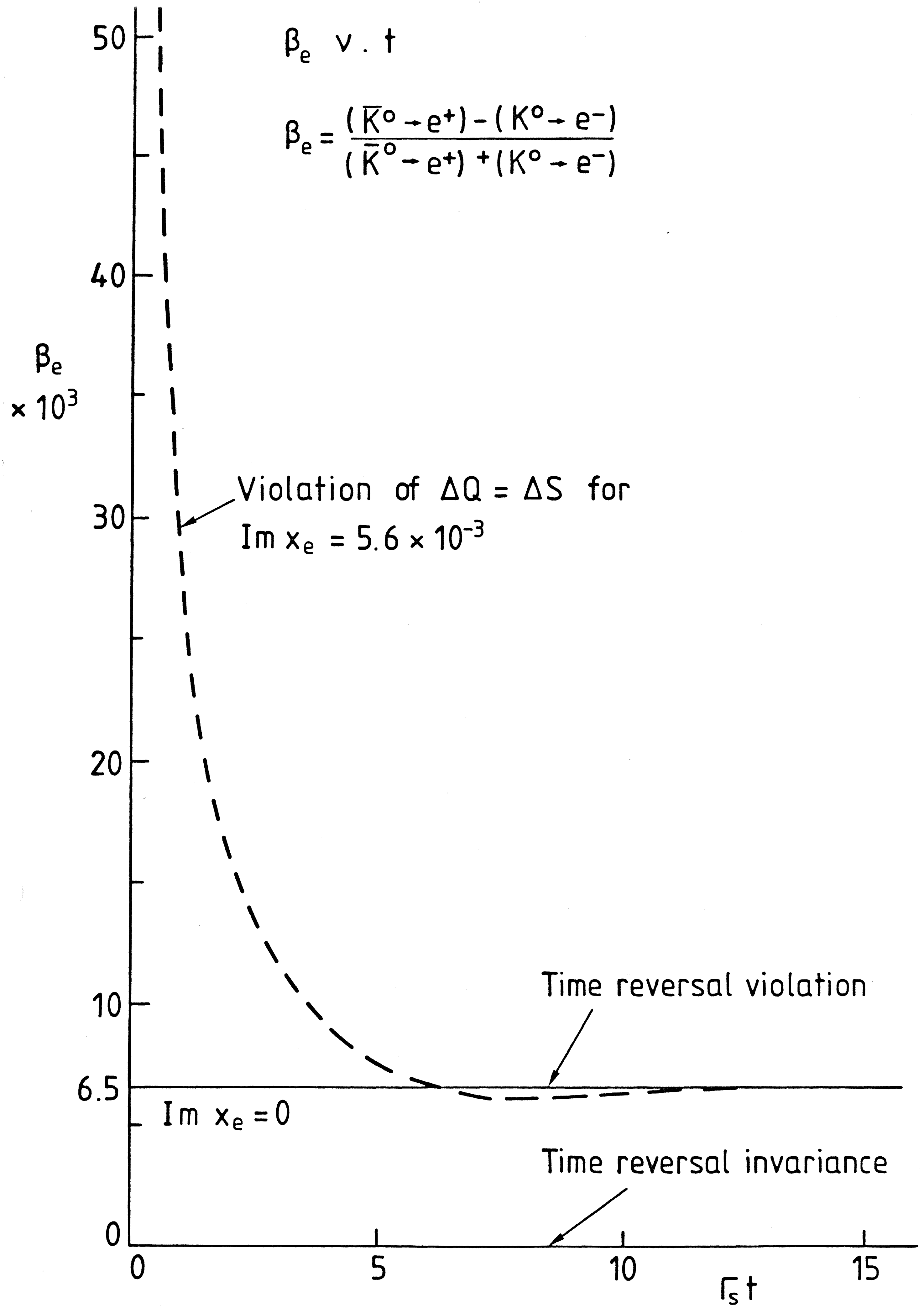

β_e v. t
$\beta_e = \frac{(\bar{K}^o \to e^+) - (K^o \to e^-)}{(\bar{K}^o \to e^+) + (K^o \to e^-)}$
$\beta_e \times 10^3$
50
40
30
20
10
6.5
0
Violation of $\Delta Q = \Delta S$ for
$\mathrm{Im}\, x_e = 5.6 \times 10^{-3}$
Time reversal violation
$\mathrm{Im}\, x_e = 0$
Time reversal invariance
0
5
10
15
$\Gamma_s t$

Fig. 4

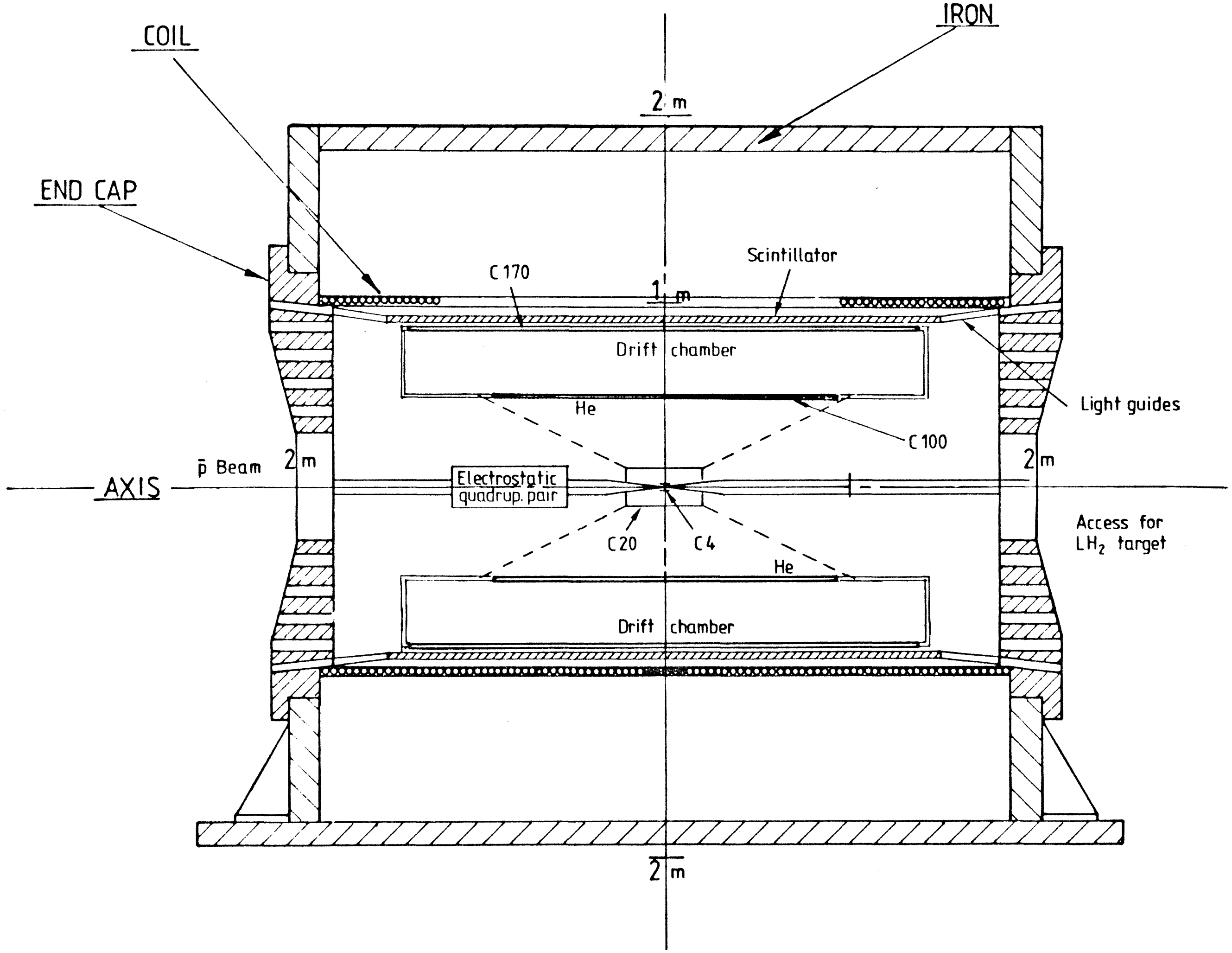
IRON
COIL
END CAP
2 m
Scintillator
C 170
1 m
Drift chamber
Light guides
He
C 100
p̄ Beam
2 m
AXIS
Electrostatic quadrup. pair
2 m
Access for
LH_2 target
C 20
C 4
He
Drift chamber
2 m

Fig. 5

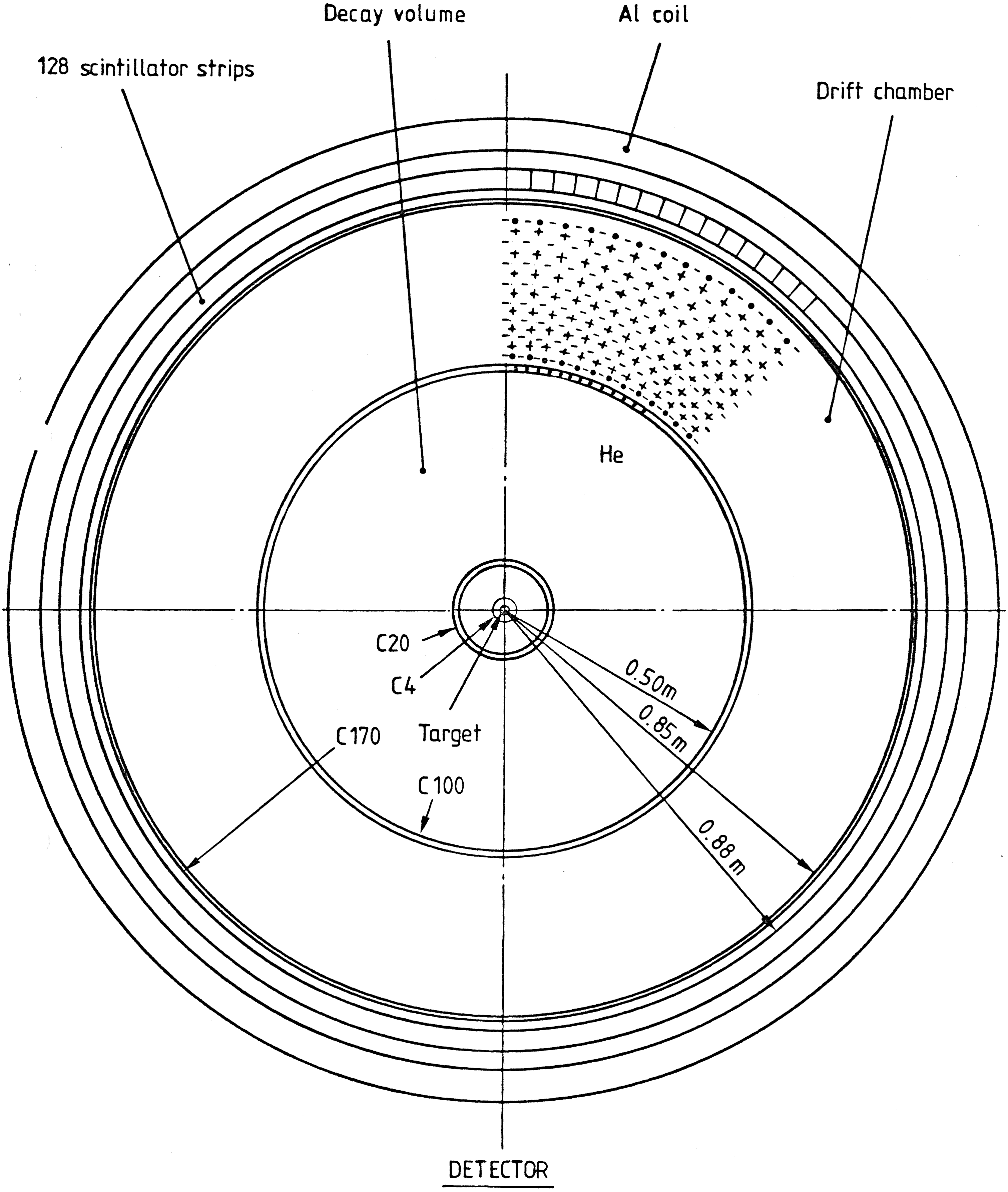
Decay volume
Al coil
128 scintillator strips
Drift chamber
He
C20
C4
Target
0.50m
0.85m
C170
C100
0.88 m
DETECTOR

Fig. 6

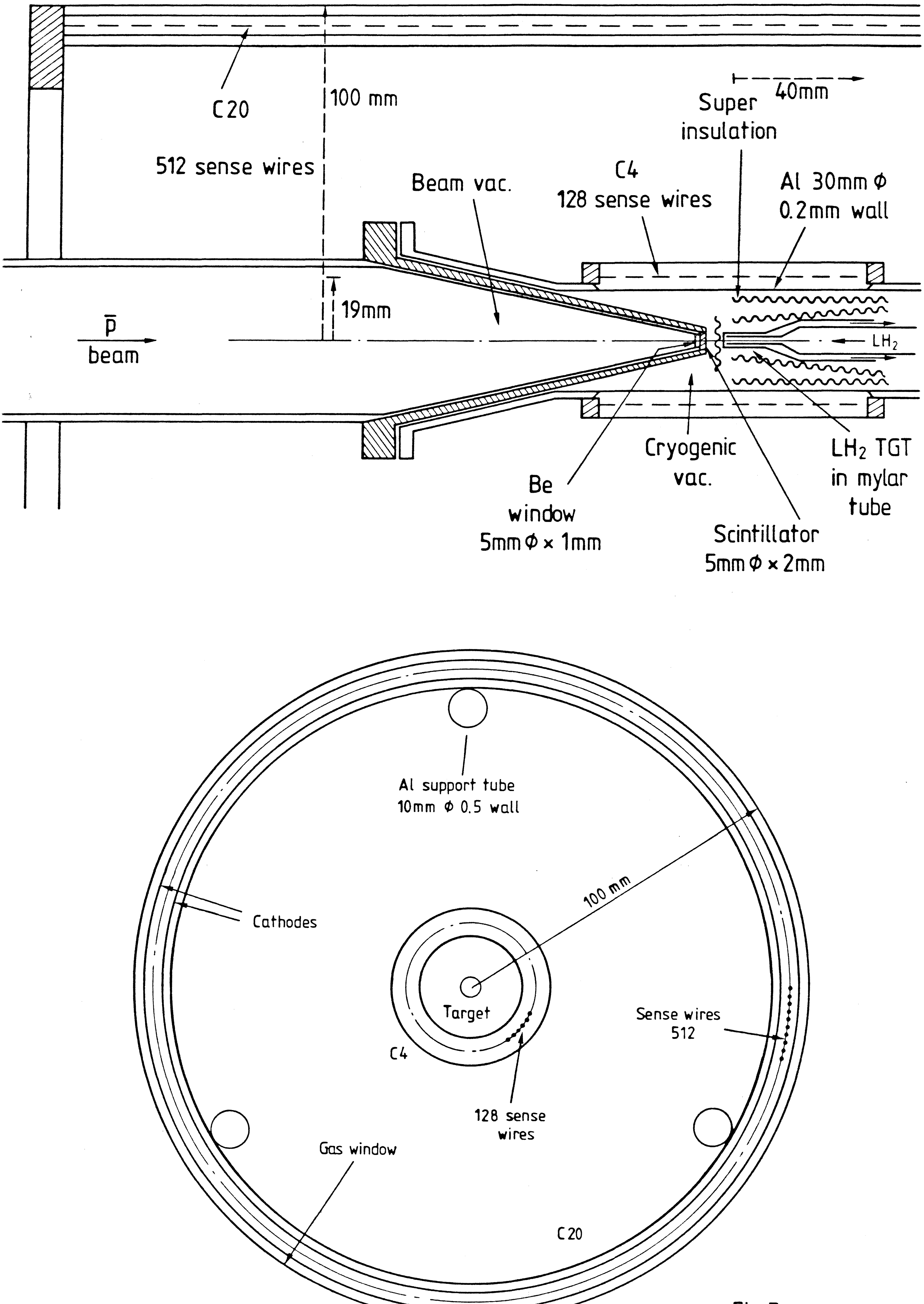
C20
512 sense wires
100 mm
19mm
$\bar{p}$
beam
Beam vac.
C4
128 sense wires
40mm
Super
insulation
Al 30mm Φ
0.2mm wall
LH_2
Be
window
5mm Φ × 1mm
Cryogenic
vac.
Scintillator
5mm Φ × 2mm
LH_2 TGT
in mylar
tube
Al support tube
10mm Φ 0.5 wall
Cathodes
100 mm
Target
C4
Sense wires
512
128 sense
wires
Gas window
C20

Fig.7

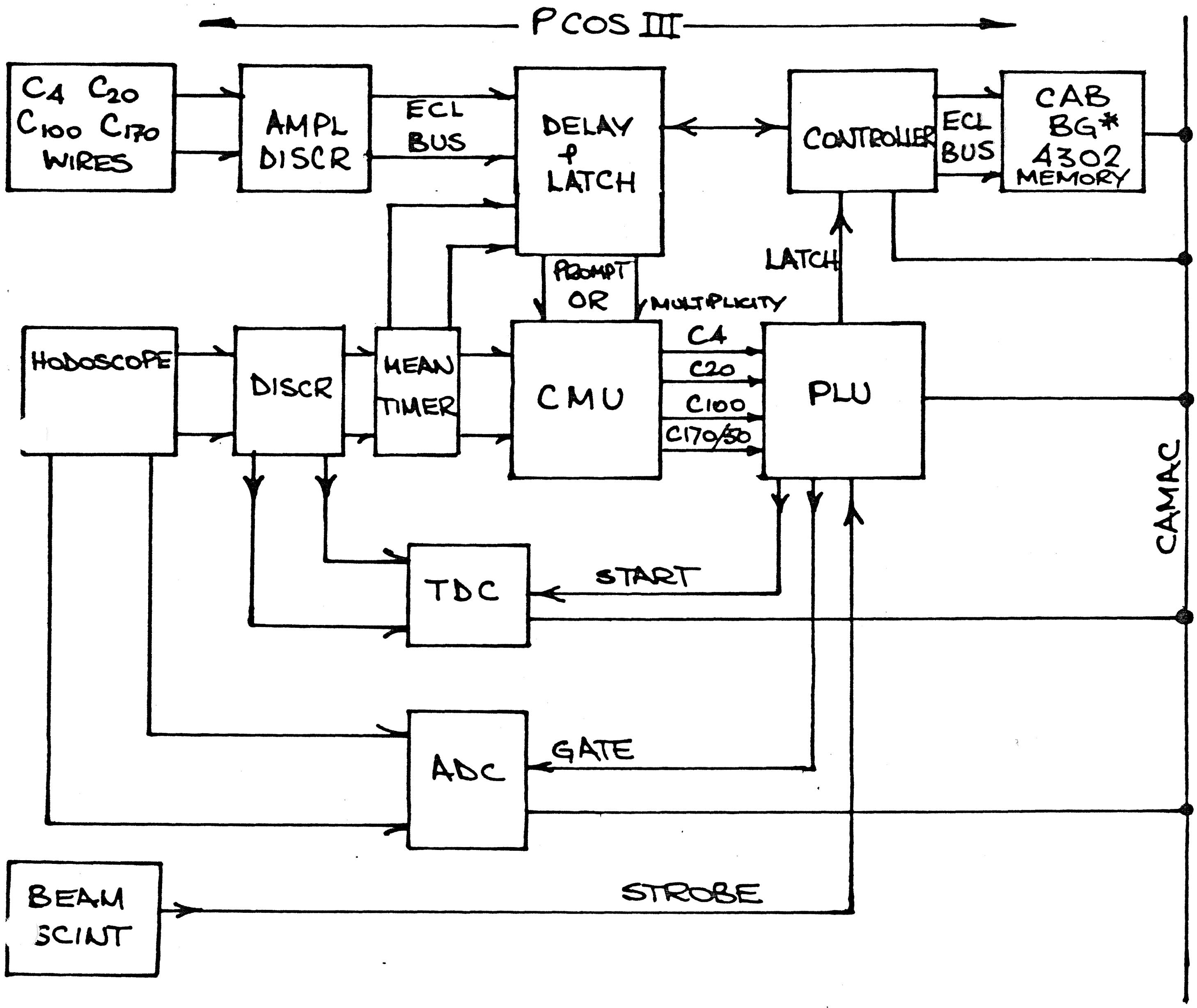
PCOS III
C4 C20
C100 C170
WIRES
AMPL
DISCR
ECL
BUS
DELAY
+
LATCH
CONTROLLER
ECL
BUS
CAB
BG*
4302
MEMORY
LATCH
PROMPT
OR
MULTIPLICITY
HODOSCOPE
DISCR
MEAN
TIMER
CMU
C4
C20
C100
C170/50
PLU
CAMAC
TDC
START
ADC
GATE
BEAM
SCINT
STROBE

FIG 8

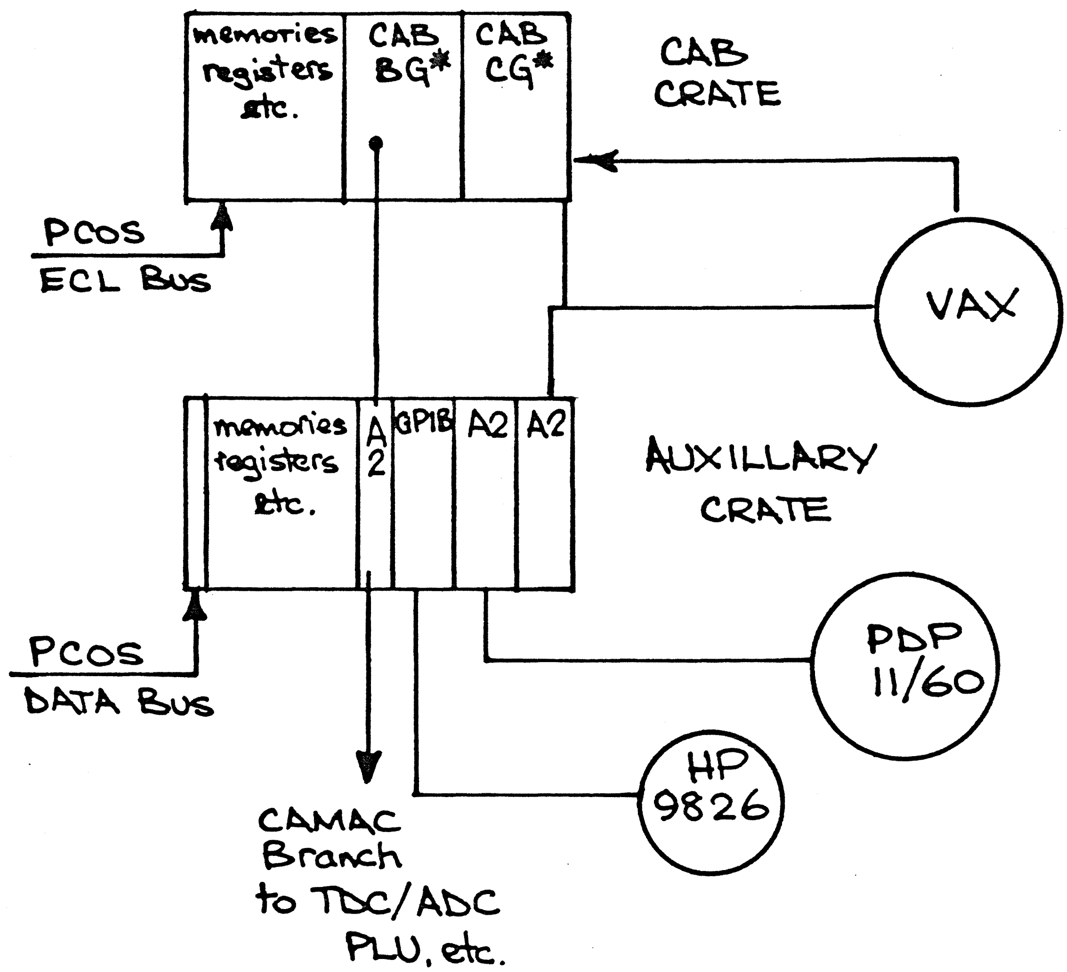
memories registers etc.
CAB BG*
CAB CG*
CAB CRATE
PCOS ECL Bus
VAX
memories registers etc.
A2
GPIB
A2
A2
AUXILLARY CRATE
PCOS DATA Bus
PDP 11/60
HP 9826
CAMAC Branch to TDC/ADC PLU, etc.

FIG 9

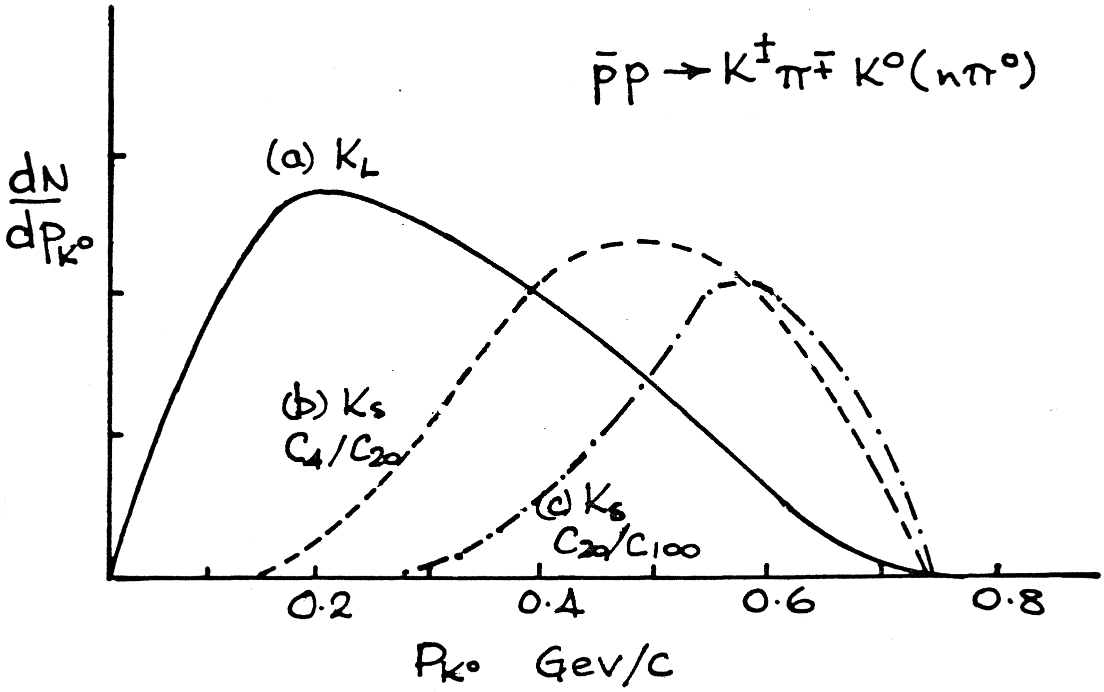
$\bar{p}p \to K^{\pm}\pi^{\mp}K^{0}(n\pi^{0})$
(a) K_L
(b) K_S
C_4/C_{20}
(c) K_S
C_{20}/C_{100}
$\frac{dN}{dp_{K^0}}$
0.2
0.4
0.6
0.8
p_{K^0} GeV/c

FIG 10

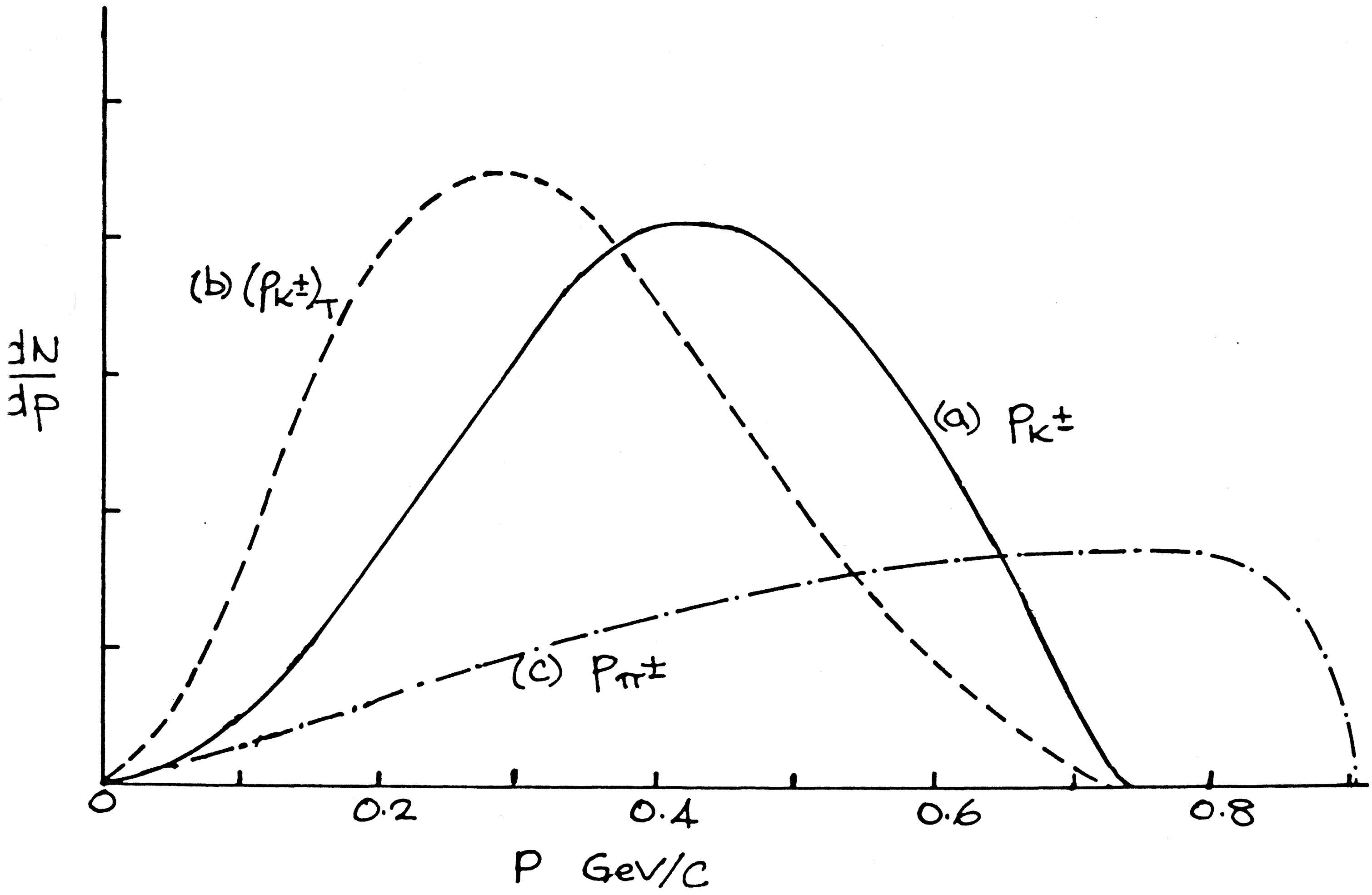
(b) $(p_{K^\pm})_T$
(a) $p_{K^\pm}$
(c) $p_{\pi^\pm}$
$\frac{dN}{dp}$
0
0.2
0.4
0.6
0.8
P GeV/c

FIG 11

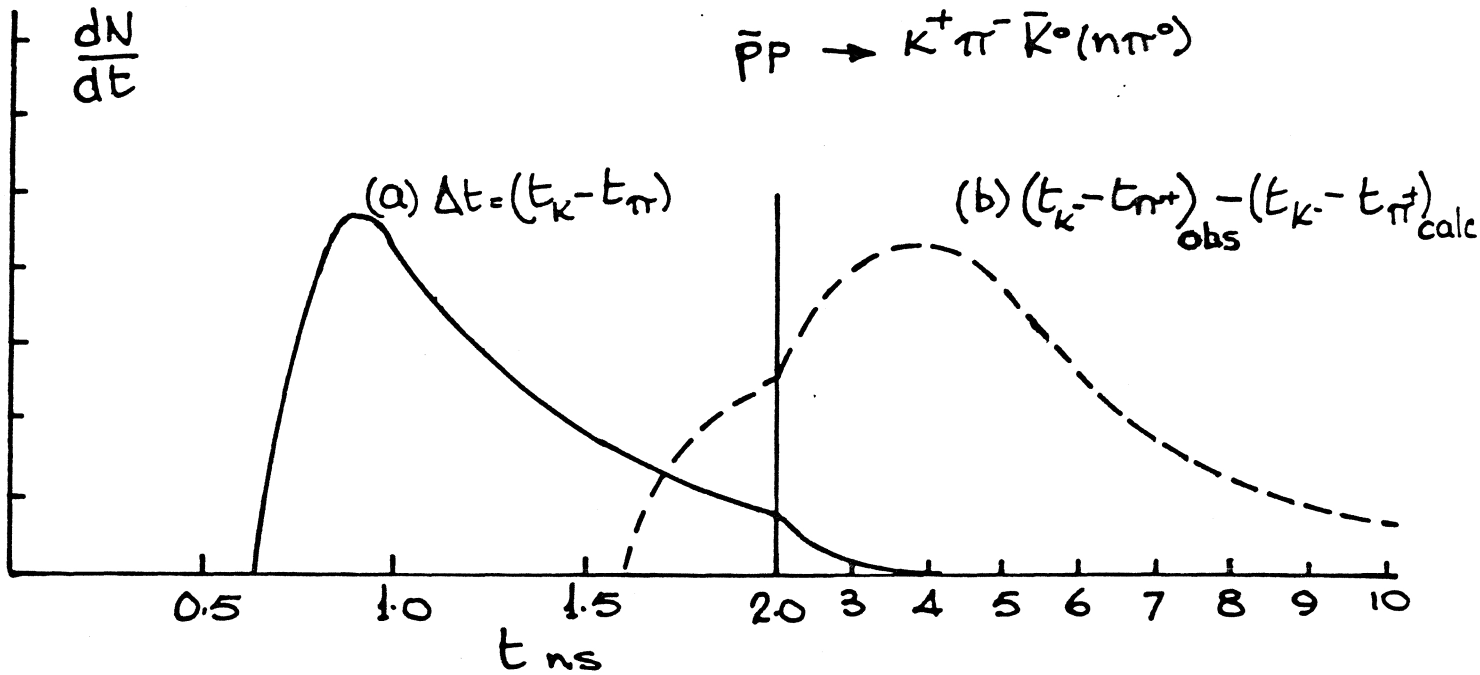

FIG 12

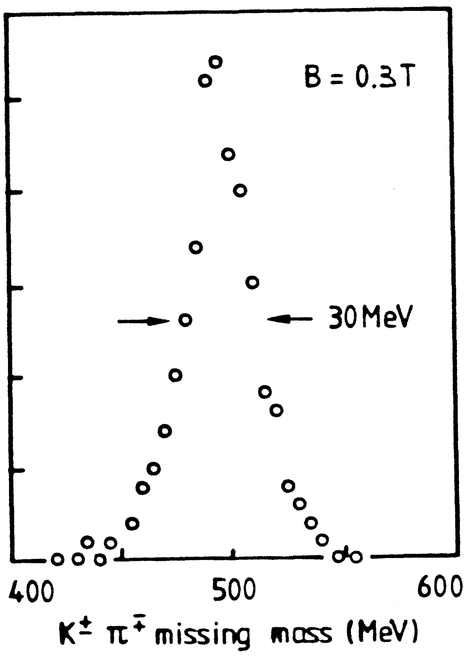

Fig. 13

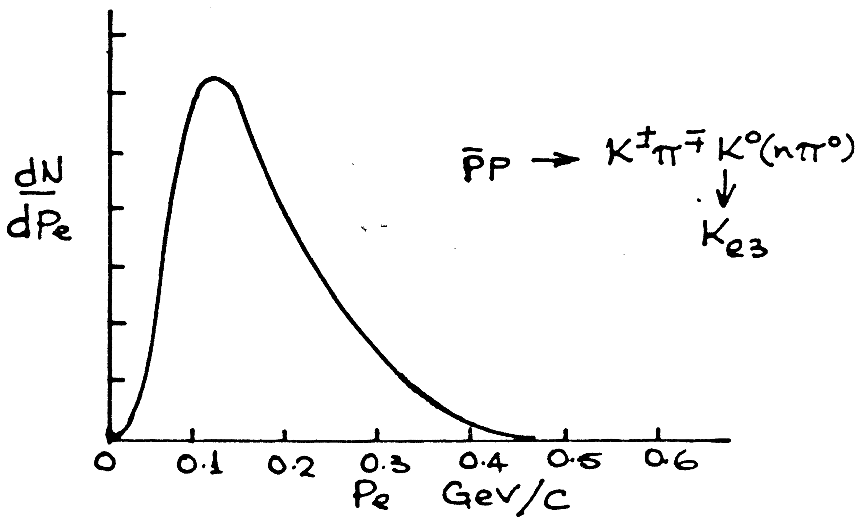

FIG 14

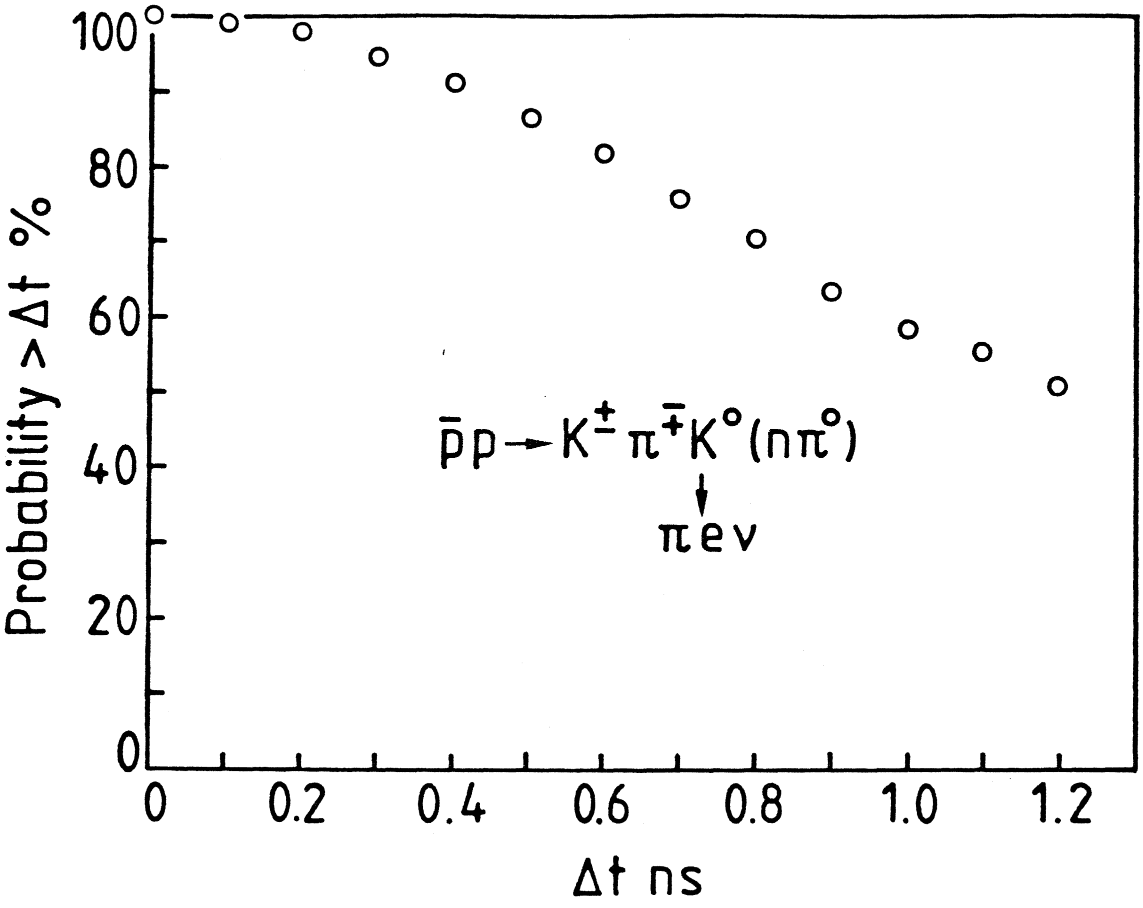

(a) $\Delta t = t_{\pi} - t_{e}$

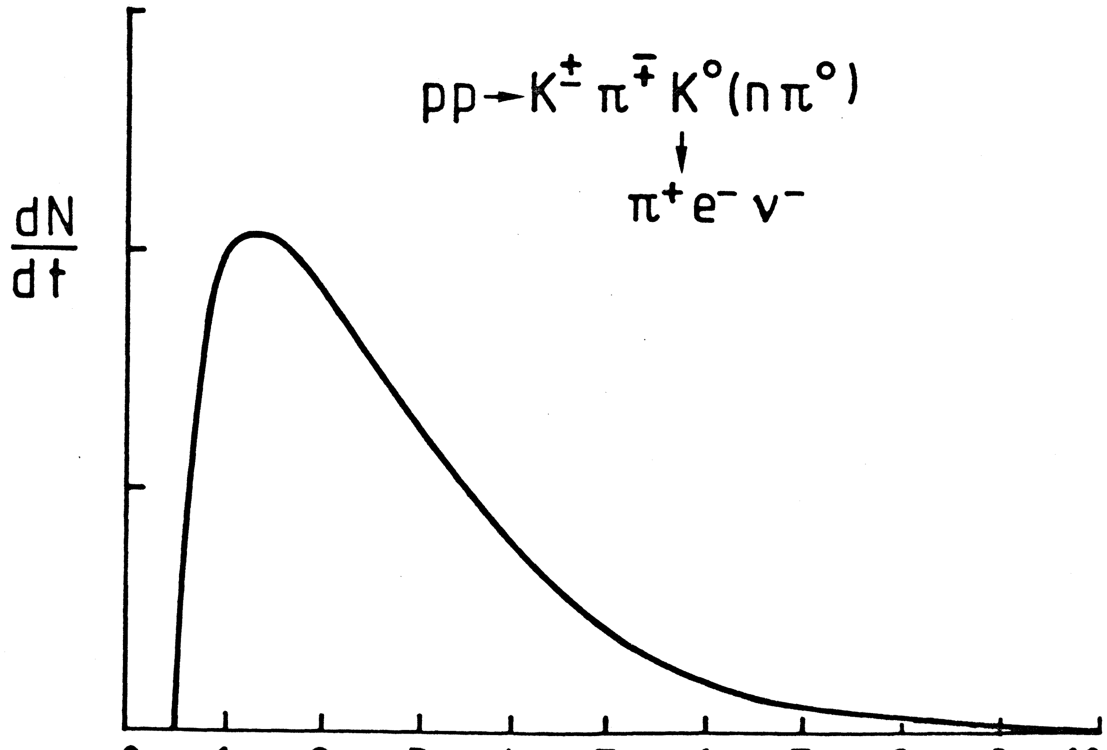

(b) $(t_{\pi^-} - t_{e^+})_{obs} - (t_{\pi^-} - t_{e^+})_{calc}$

Fig. 15

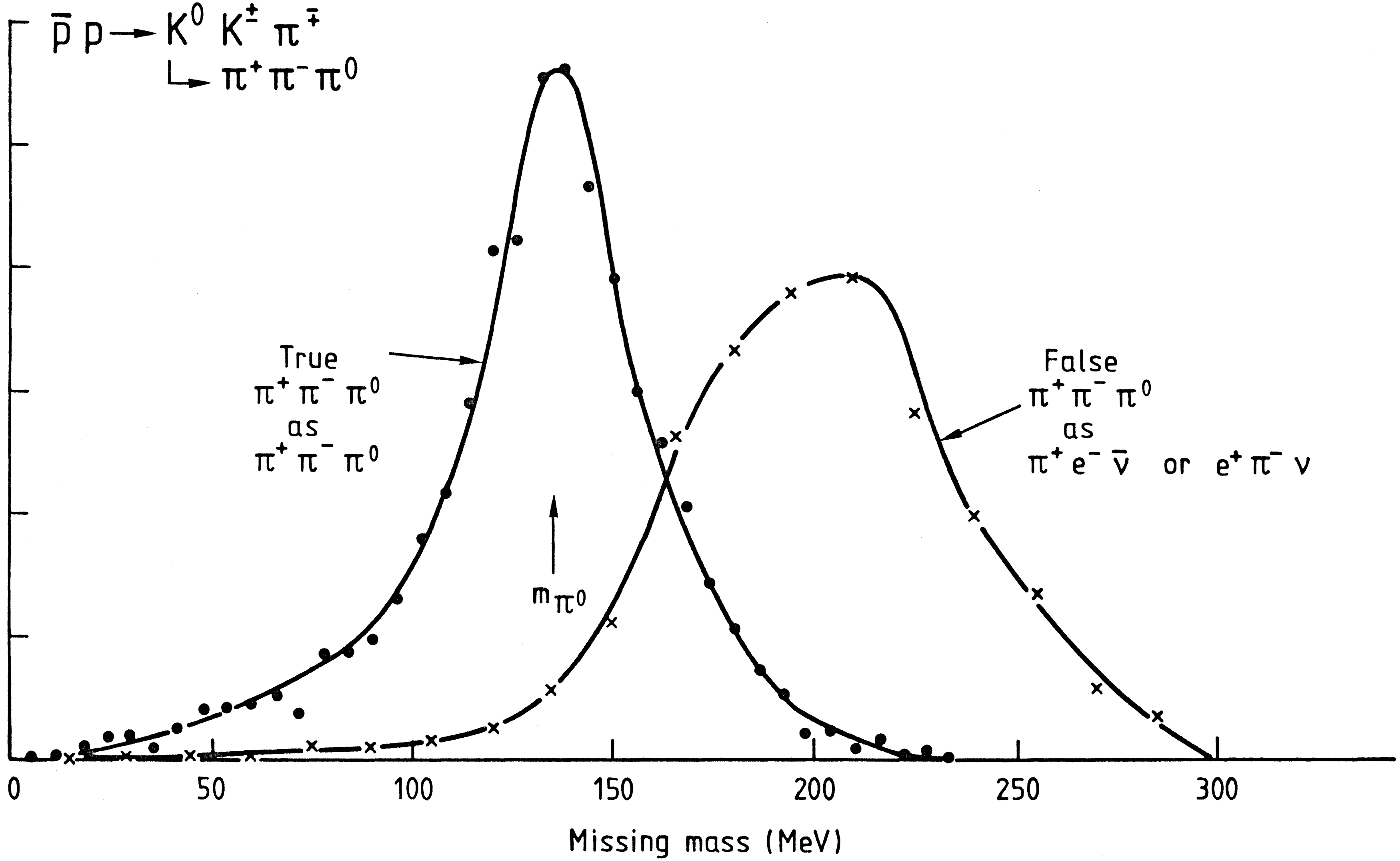

$\bar{p}p \to K^0 K^{\pm} \pi^{\mp}$
$\hookrightarrow \pi^+\pi^-\pi^0$
True
$\pi^+\pi^-\pi^0$
as
$\pi^+\pi^-\pi^0$
False
$\pi^+\pi^-\pi^0$
as
$\pi^+e^-\bar{\nu}$ or $e^+\pi^-\nu$
m_{π^0}
0
50
100
150
200
250
300
Missing mass (MeV)

Fig.16